J. Fluid Mech. (1994), *vol.* 265, *pp.* 303–343

Resonant capillary–gravity interfacial waves

By P. CHRISTODOULIDES AND F. DIAS

Institut Non-Linéaire de Nice, UMR 129 CNRS, 1361 route des Lucioles, 06560 Valbonne, France

(Received 22 February 1993 and in revised form 22 June 1993)

Two-dimensional space-periodic capillary–gravity waves at the interface between two fluids of different densities are considered when the second harmonic and the fundamental mode are near resonance. A weakly nonlinear analysis provides the equations (normal form), correct to third order, that relate the wave frequency with the amplitudes of the fundamental mode and of the second harmonic for all waves with small energy. A study of the normal form for waves which are also periodic in time reveals three possible types of space- and time-periodic waves: the well-known travelling and standing waves as well as an unusual class of three-mode mixed waves. Mixed waves are found to provide a connection between standing and travelling waves. The branching behaviour of all types of waves is shown to depend strongly on the density ratio. For travelling waves the weakly nonlinear results are confirmed numerically and extended to finite-amplitude waves. When slow modulations in time of the amplitudes are considered, a powerful geometrical method is used to study the resulting normal form. Finally a discussion on modulational stability suggests that increasing the density ratio has a stabilizing effect.

1. Introduction

Our purpose here is to study in detail all types of two-dimensional space- and time-periodic capillary–gravity interfacial waves when the second harmonic resonates with the fundamental mode. Such a resonance has been thoroughly studied in the case of travelling water waves. However, considering all types of space- and time-periodic waves and including the density ratio as an extra parameter reveal new results.

To begin, consider a two-dimensional capillary–gravity interfacial wave, which is periodic in space with wavenumber k and in time with frequency ω. Both fluids are supposed to be of infinite depth. A dimensionless parameter which is commonly used to define the relative importance of gravity and surface tension is the number

$$b = \frac{k^2\sigma}{(\rho - \rho')g}, \tag{1.1}$$

where σ is the surface tension at the interface, ρ is the density of the lower fluid, ρ' is the density of the upper fluid and g is the acceleration due to gravity.

When $b = \frac{1}{2}$, the fundamental mode and the second harmonic are resonantly coupled. A natural way to explain this phenomenon is to consider the linearization of the interfacial wave problem. The wavenumber k and the linear frequency ω_0 must then satisfy the linear dispersion relation

$$\omega_0^2 = \varrho g k(1 + b), \tag{1.2}$$

where

$$\varrho = (\rho - \rho')/(\rho + \rho'). \tag{1.3}$$

If nonlinear terms are included in the equations, the quadratic terms excite time-independent and second-harmonic components of wavenumber $2k$ and frequency $2\omega_0$. In general, the fundamental mode and the second harmonic are uncoupled, but if the wavenumber $2k$ and the frequency $2\omega_0$ also satisfy the dispersion relation (1.2) the two modes resonate and their amplitudes are of the same order of magnitude. Such resonance occurs only if $b = \frac{1}{2}$.

Waves characterized by two dominant modes are often called Wilton's ripples in the literature in reference to Wilton's (1915) paper. It turns out that the phenomenon described as Wilton's ripples was discussed at least twice prior to Wilton's paper: in an unpublished addendum to an essay that Bohr (1906) wrote in order to win the Royal Danish Academy Prize on the theme 'The surface tension of water' and in a paper by Harrison (1909).

The references mentioned in this paragraph all deal with water waves. Pierson & Fife (1961) studied travelling Wilton's ripples in infinite depth by using a classical perturbation expansion of the elevation of the interface η, the velocity potential ϕ and the phase velocity of the wave c, which they modified accordingly when $b = \frac{1}{2}$. Their analysis is valid up to second order (except for a constant that they did not compute). They also did a wavenumber perturbation analysis to study waves with wavenumbers close but not equal to the wavenumber corresponding to $b = \frac{1}{2}$. Barakat & Houston (1968) extended the analysis of Pierson & Fife to finite depth while Nayfeh (1970) extended the results of Barakat & Houston to third order. Simmons (1969) and McGoldrick (1970*b*) analysed Wilton's ripples and their dynamics in the more general framework of resonant wave interactions. Simmons, whose analysis is based on a variational method and McGoldrick, whose analysis is based on the method of multiple time and space scales, both obtained equations for slow modulations in space and in time of the amplitudes of the fundamental mode and of the second harmonic. McGoldrick (1970*b*) showed that Wilton's ripples are in fact solutions to the amplitude equations for special initial values. Standing Wilton's ripples have been considered by Vanden-Broeck (1984) through a classical perturbation analysis. Chen & Saffman (1979) studied the more general problem of travelling waves with two dominant modes by using a formal perturbation procedure. They showed that the Wilton's ripple phenomenon is in fact associated with a bifurcation in which a wave of permanent form can double its period, and that so-called combination (M, N) waves are possible for all sets of positive integers M and N for appropriate values of b. Reeder & Shinbrot (1981*a*) transformed the fluid domain into a fixed one and studied Wilton's ripples both in two and three dimensions. Reeder & Shinbrot (1981*b*) provided the first rigorous theory of Wilton's ripples. Toland & Jones (1985) and Jones & Toland (1986) used an integral equation formulation of the water-wave problem and gave a systematic description of combination waves as an aspect of bifurcation theory in the presence of symmetries. They reduced the problem by the Lyapunov–Schmidt procedure. Jones (1989) extended the previous work to waves in finite water depth. Aston (1991) considered the structure of combination $(1, N)$ waves with N larger than four. He studied the effect of higher-order terms in the bifurcation equations. Aston (1993) attempted an extensive description of the amazingly large number of travelling wave solutions to the capillary–gravity wave problem by following two-parameter paths of turning and bifurcation points which

originate at the trivial solution at points of mode interaction. Bridges (1990) based his study of all space- and time-periodic combination waves on their symmetries and on the Hamiltonian structure of the water-wave problem. The idea of considering all types of periodic waves, and not travelling waves nor standing waves in isolation, goes back to Rayleigh (1915). In the no-resonance case, Rayleigh showed that indeed there are only two possible types of space- and time-periodic waves: travelling waves and standing waves. In the case where two modes resonate, Bridges (1990) showed that in addition to well-known travelling and standing waves other classes of periodic waves, in particular three-mode mixed waves, may exist. Our analysis includes such waves for the 1:2 resonance.

McGoldrick's (1970*b*) results for water waves have been extended to travelling interfacial waves by Nayfeh & Saric (1972). Bontozoglou & Hanratty (1990) used the variational method developed by Miles (1986) to extend the results to third order for periodic waves without the inclusion of time and space modulations.

Numerical results for waves near resonance include those of Schwartz & Vanden-Broeck (1979), Chen & Saffman (1980), Vanden-Broeck (1980*a*), Hogan (1981), Vanden-Broeck (1984) for standing waves, and Vanden-Broeck (1980*b*) and Bontozoglou & Hanratty (1990) for interfacial waves.

The stability of travelling capillary–gravity waves has been studied extensively. It is well-known that the modulations of a train of weakly nonlinear waves in deep water are governed by a nonlinear Schrödinger equation, which can be derived for example by the method of multiple scales in time and in space (Kawahara 1975; Djordjevic & Redekopp 1977). However, the derivation is invalid near the second-harmonic resonance. McGoldrick (1970*b*) obtained a system of two equations governing the space and time modulations of travelling Wilton's ripples (at order two). These equations, which also appear in other physical systems, have been studied in detail (see Craik 1985 for a review). Jones (1992) used the method of multiple scales to extend McGoldrick's work to third order and obtained a pair of coupled nonlinear partial differential equations, which he solved only for special cases (periodic solutions). The nonlinear Schrödinger equation admits several types of analytical solutions (see Peregrine 1983 for a review). To our knowledge, analytical solutions to Jones' coupled equations have not been studied yet. The stability of gravity interfacial waves has also been studied (see Grimshaw & Pullin 1985 for analytical results based on a multiple scale expansion, Pullin & Grimshaw 1985 for numerical results, Dixon 1990 and Zhou, Lee & Cheung 1992 for results based on the Zakharov equation). Nayfeh & Saric (1972) conducted a nonlinear stability analysis of capillary–gravity interfacial waves by using the method of multiple scales.

Travelling Wilton's ripples have been observed experimentally (McGoldrick 1970*a*; Henderson & Hammack 1987; Perlin & Hammack 1991) and it appears that the 1:2 internal resonance can be excited by waves with surprisingly small steepnesses. A detailed description of the experiments can be found in the review article by Hammack & Henderson (1993). Perlin & Ting (1992) performed systematic experiments in the 1:2 resonance regime. In their conclusions, they state that 'the experimental results (symmetric part) are in general agreement with the results of Schwartz & Vanden-Broeck and Chen & Saffman.' All the above experiments are concerned with water waves. Capillary–gravity interfacial waves have also been studied experimentally, especially in relation to the Kelvin–Helmholtz instability. The importance of the 1:2 resonance in gas–liquid flows has been emphasized by Bontozoglou & Hanratty (1990). Experiments by Thorpe (1969) and Pouliquen *et al.* (1992) show that surface tension can be an important factor for waves propagating at the interface between

two fluids with almost the same density and that viscous dissipation can be negligible under certain circumstances.

The problem is formulated in § 2. A weakly nonlinear analysis provides the normal form (truncated at third order), i.e. the equations relating the frequency to the amplitudes of the wave, valid for all space- and time-periodic waves with small energy. The normal form is studied for each class of periodic waves (travelling waves in § 3, standing waves in § 5 and mixed waves in § 6). The analysis is performed first at exact resonance ($b = \frac{1}{2}$) and then near resonance (b in a neighbourhood of $\frac{1}{2}$). The density ratio is shown to play an important role. In particular, if the ratio is close to one, the behaviour of travelling or standing Wilton's ripples is more complicated than in the water-wave case because of the existence of several bifurcations. The analysis also reveals the existence of several branches of mixed waves which connect branches of travelling and standing waves. Finite-amplitude travelling waves are computed numerically in § 4. In § 7, a powerful geometrical method, which has been recently applied to the study of dynamical systems with symmetries, is used to analyse the effects of slow modulations in time of the wave amplitudes. A discussion on stability, dissipation and experiments in relation to resonant capillary–gravity interfacial waves is given in § 8.

2. Problem formulation and weakly nonlinear analysis

A fluid of density ρ' lies on top of a heavier fluid of density ρ. The line $y = 0$ represents the interface at rest. When in motion, the interface is described by $y = \eta(x, t)$, where x denotes the horizontal coordinate. Both fluids are inviscid and incompressible. The flows in each fluid are assumed to be two-dimensional and irrotational. Therefore, velocity potentials are introduced in each fluid. The governing equations are given by

$$\nabla \cdot \vec{u} = \nabla^2 \phi = 0, \qquad \nabla \cdot \vec{u}' = \nabla^2 \phi' = 0, \tag{2.1}$$

where $\vec{u}$ and $\vec{u}'$ are the velocities of the lower and upper fluids respectively, generated by corresponding potentials ϕ and ϕ', subject to the conditions

$$\lim_{y \to -\infty} |\nabla \phi| = 0, \qquad \lim_{y \to +\infty} |\nabla \phi'| = 0. \tag{2.2}$$

At the interface $y = \eta(x, t)$, the kinematic and dynamic conditions are given by

$$\eta_t = \Phi_{(y)} - \eta_x \Phi_{(x)} = \Phi'_{(y)} - \eta_x \Phi_{(x)}, \tag{2.3}$$

and

$$\rho \left(\Phi_{(t)} + \tfrac{1}{2} |\boldsymbol{u}|^2 \right) - \rho' \left(\Phi'_{(t)} + \tfrac{1}{2} |\boldsymbol{u}'|^2 \right) + g(\rho - \rho')\eta - \sigma \frac{\eta_{xx}}{(1 + \eta_x^2)^{\frac{3}{2}}} = 0, \tag{2.4}$$

where $\Phi_{(*)} = \phi_{(*)}(x, \eta, t)$, $\Phi'_{(*)} = \phi'_{(*)}(x, \eta, t)$, $\boldsymbol{u} = \vec{u}(x, \eta, t)$, $\boldsymbol{u}' = \vec{u}'(x, \eta, t)$.

The above problem has a Hamiltonian formulation (Benjamin & Bridges 1991) given by

$$\eta_t = \delta H(\zeta, \eta)/\delta \zeta, \qquad \zeta_t = -\delta H(\zeta, \eta)/\delta \eta, \tag{2.5}$$

with the derivatives δ as variational derivatives. The canonical variable ζ in (2.5) is equal to $\rho\Phi - \rho'\Phi'$. The Hamiltonian H is the sum of the kinetic energy

$$K(\phi, \phi', \eta) = \int_0^L \left[\int_{-\infty}^{\eta} \tfrac{1}{2} \rho |\nabla \phi|^2 \, \mathrm{d}y + \int_{\eta}^{+\infty} \tfrac{1}{2} \rho' |\nabla \phi'|^2 \, \mathrm{d}y \right] \mathrm{d}x \tag{2.6}$$

and of the potential energy

$$V(\eta) = \int_0^L \left[\tfrac{1}{2}(\rho - \rho')g\eta^2 + \sigma\left(\left(1+\eta_x^2\right)^{\frac{1}{2}} - 1\right)\right] \mathrm{d}x. \tag{2.7}$$

Spatial periodicity with wavelength L and wavenumber $k = 2\pi/L$ is assumed in the x-direction. In (2.6), the kinetic energy is given as a function of ϕ and ϕ'. To prove that ϕ and ϕ' only appear in the combination ζ can be done by using the calculus of variations. That is, $K(\zeta,\eta)$ is obtained as the minimum of $K(\phi,\phi',\eta)$ with η fixed on the constant set $\rho\Phi - \rho'\Phi' = \zeta$.

The above Hamiltonian formulation has an equivalent Lagrangian formulation: the set of equations (2.5) can be recovered from setting the first variation of

$$\mathscr{L} = \int_{t_1}^{t_2} (K(\eta_t,\eta) - V(\eta))\, \mathrm{d}t \tag{2.8}$$

equal to zero. The link between η_t and ζ is provided by

$$\eta_t = \delta K(\zeta,\eta)/\delta\zeta\,. \tag{2.9}$$

With the restriction to space- and time-periodic functions, the canonical variables $\eta(x,t)$ and $\zeta(x,t)$ can be formally identified with a double Fourier series expansion in x and in t. For computational purposes, the Fourier series are restricted to N terms. In Appendix A, we show how to compute $K(\zeta,\eta)$ in terms of the Fourier coefficients of the expansions of ζ and η in x, and how to eliminate ζ in order to obtain $K(\eta_t,\eta)$. For the weakly nonlinear analysis performed in this paper, it is sufficient to take $N = 4$. In Appendix A, the Lagrangian $K - V$ is also computed and integrated over a time period to give the functional $\mathscr{L}$. The coefficients of the third and fourth harmonic are then eliminated. Dimensionless variables are introduced by choosing $1/k$ as unit length and $(gk)^{\frac{1}{2}}$ as unit frequency. The resulting expression for $\mathscr{L}$, which has been divided by

$$\pi^2(\rho + \rho')gk^{-3}\omega^{-1}(gk)^{-\frac{1}{2}}\,, \tag{2.10}$$

where ω now denotes the dimensionless frequency, is

$$\begin{aligned}\mathscr{L} = {} & \left(\omega^2 - \varrho(1+b)\right)E_1 + \left(2\omega^2 - \varrho(1+4b)\right)E_2 - \tfrac{1}{2}\varrho\omega^2 S \\ & - \varrho\left[\alpha_{11}E_1^2 + \beta_{11}M_1^2 + \alpha_{22}E_2^2 + \beta_{22}M_2^2 + 2\alpha_{12}E_1E_2 + 2\beta_{12}M_1M_2\right] + \cdots .\end{aligned} \tag{2.11}$$

The dots denote higher-order terms. The full expressions for the coefficients α_{ij} and β_{ij}, which depend on b (1.1), ϱ (1.3) and ω^2, can be found in Appendix B. The quantities E_1, E_2, M_1, M_2, S are given by

$$E_i = |A_i|^2 + |B_i|^2 \qquad (i = 1,2), \tag{2.12}$$

$$M_i = |B_i|^2 - |A_i|^2 \qquad (i = 1,2), \tag{2.13}$$

$$S = A_1^2\overline{A_2} + \overline{A_1}^2 A_2 + B_1^2\overline{B_2} + \overline{B_1}^2 B_2\,, \tag{2.14}$$

where the coefficients A_i and B_i are the first-order complex Fourier coefficients of

$$\eta = \mathrm{Re}\left[A_1 \mathrm{e}^{-\mathrm{i}(\omega t - x)} + B_1 \mathrm{e}^{-\mathrm{i}(\omega t + x)} + A_2 \mathrm{e}^{-\mathrm{i}(2\omega t - 2x)} + B_2 \mathrm{e}^{-\mathrm{i}(2\omega t + 2x)} + \cdots\right]. \tag{2.15}$$

The fact that the amplitudes A_i and B_i only appear in the combinations E_i, M_i and S comes from the symmetries of the problem. In fact Bridges (1990) obtained the expression for $\mathscr{L}$ simply by considering the symmetries of the water-wave problem, without using the equations. But the equations of the problem are of course needed in order to compute the values of the coefficients in terms of the physical parameters.

The normal form, i.e. the system of equations that relates the complex amplitudes A_1, B_1, A_2, B_2 to the angular frequency ω, is obtained by setting the derivatives of $\mathscr{L}$ in (2.11) with respect to A_1, B_1, A_2, B_2 and their conjugates to zero. We obtain eight equations but only four are listed below (since the other four are their complex conjugates):

$$\left.\begin{aligned}
&\left(\omega^2 - \varrho(1+b)\right) A_1 - \varrho\omega^2 \overline{A_1} A_2 - 2\varrho A_1 \left(\alpha_{11}E_1 - \beta_{11}M_1 + \alpha_{12}E_2 - \beta_{12}M_2\right) + \cdots = 0,\\
&\left(\omega^2 - \varrho(1+b)\right) B_1 - \varrho\omega^2 \overline{B_1} B_2 - 2\varrho B_1 \left(\alpha_{11}E_1 + \beta_{11}M_1 + \alpha_{12}E_2 + \beta_{12}M_2\right) + \cdots = 0,\\
&\left(2\omega^2 - \varrho(1+4b)\right) A_2 - \tfrac{1}{2}\varrho\omega^2 A_1^2 - 2\varrho A_2 \left(\alpha_{12}E_1 - \beta_{12}M_1 + \alpha_{22}E_2 - \beta_{22}M_2\right) + \cdots = 0,\\
&\left(2\omega^2 - \varrho(1+4b)\right) B_2 - \tfrac{1}{2}\varrho\omega^2 B_1^2 - 2\varrho B_2 \left(\alpha_{12}E_1 + \beta_{12}M_1 + \alpha_{22}E_2 + \beta_{22}M_2\right) + \cdots = 0.
\end{aligned}\right\} \tag{2.16}$$

Similar equations restricted to travelling waves have been obtained previously by Nayfeh (1970) and Bontozoglou & Hanratty (1990). The system of equations (2.16) can be used to compute $\mathscr{L}$ at the stationary points corresponding to the periodic solutions. One finds

$$\mathscr{L} = \tfrac{1}{4}\varrho\omega^2 S + \varrho\left[\alpha_{11}E_1^2 + \beta_{11}M_1^2 + \alpha_{22}E_2^2 + \beta_{22}M_2^2 + 2\alpha_{12}E_1E_2 + 2\beta_{12}M_1M_2\right] + \cdots .$$

The total energy $\mathscr{H}$, equal to the integral over a time period of the Hamiltonian H, is (after being divided by 2.10)

$$\begin{aligned}
\mathscr{H} = {} & 2\varrho(1+b)E_1 + 2\varrho(1+4b)E_2 + \tfrac{1}{4}\varrho\omega^2 S\\
& + \varrho\left[\alpha_{11}^H E_1^2 + \beta_{11}^H M_1^2 + \alpha_{22}^H E_2^2 + \beta_{22}^H M_2^2 + 2\alpha_{12}^H E_1E_2 + 2\beta_{12}^H M_1M_2\right] + \cdots ,
\end{aligned} \tag{2.17}$$

where the expressions for the coefficients α_{ij}^H and β_{ij}^H appearing inside the brackets can be found in Appendix C.

The normal form (2.16) for all periodic solutions can be rewritten in terms of amplitude and phase. Letting $A_i = a_i e^{i\varphi_i^a}$, $B_i = b_i e^{i\varphi_i^b}$ yields

$$\left.\begin{aligned}
&\left(\omega^2 - \varrho(1+b)\right) a_1 \mp \varrho\omega^2 a_1 a_2 - 2\varrho a_1 \left(\alpha_{11}E_1 - \beta_{11}M_1 + \alpha_{12}E_2 - \beta_{12}M_2\right) + \cdots = 0,\\
&\left(\omega^2 - \varrho(1+b)\right) b_1 \mp \varrho\omega^2 b_1 b_2 - 2\varrho b_1 \left(\alpha_{11}E_1 + \beta_{11}M_1 + \alpha_{12}E_2 + \beta_{12}M_2\right) + \cdots = 0,\\
&\left(2\omega^2 - \varrho(1+4b)\right) a_2 \mp \tfrac{1}{2}\varrho\omega^2 a_1^2 - 2\varrho a_2 \left(\alpha_{12}E_1 - \beta_{12}M_1 + \alpha_{22}E_2 - \beta_{22}M_2\right) + \cdots = 0,\\
&\left(2\omega^2 - \varrho(1+4b)\right) b_2 \mp \tfrac{1}{2}\varrho\omega^2 b_1^2 - 2\varrho b_2 \left(\alpha_{12}E_1 + \beta_{12}M_1 + \alpha_{22}E_2 + \beta_{22}M_2\right) + \cdots = 0.
\end{aligned}\right\} \tag{2.18}$$

In the first and third equations, the minus sign must be used if $\cos(\varphi_2^a - 2\varphi_1^a) = 1$ while the plus sign must be used if $\cos(\varphi_2^a - 2\varphi_1^a) = -1$. In the second and fourth equations, the minus sign must be used if $\cos(\varphi_2^b - 2\varphi_1^b) = 1$ while the plus sign must be used if $\cos(\varphi_2^b - 2\varphi_1^b) = -1$.

A look at the linearization of the normal form,

$$\left(\omega_0^2 - \varrho(1+b)\right)\begin{pmatrix} A_1 \\ B_1 \end{pmatrix} = \begin{pmatrix} 0 \\ 0 \end{pmatrix}, \qquad \left(2\omega_0^2 - \varrho(1+4b)\right)\begin{pmatrix} A_2 \\ B_2 \end{pmatrix} = \begin{pmatrix} 0 \\ 0 \end{pmatrix},$$

where ω_0 denotes the linear frequency, shows that there are three cases to consider besides the trivial solution $(A_1, B_1, A_2, B_2) = (0,0,0,0)$: 1-waves, (1,2)-waves and 2-waves.

(a) Reduction for 1-waves

This case corresponds to $\omega_0^2 = \varrho(1+b)$ while $2\omega_0^2 \neq \varrho(1+4b)$. In the linearization, the coefficients of the second harmonic must be zero, which explains the terminology

1-wave. If quadratic terms are added, the third and fourth equations of the normal form (2.16) show that the coefficients A_2 and B_2 of the second harmonic are of the order of the square of the coefficients A_1 and B_1 of the fundamental mode:

$$A_2 = \frac{1+b}{2(1-2b)}\varrho A_1^2 + \cdots, \qquad B_2 = \frac{1+b}{2(1-2b)}\varrho B_1^2 + \cdots,$$

where ω^2 has been replaced by ω_0^2. Replacing A_2 and B_2 in the first two equations modifies the coefficients of $A_1|A_1|^2$ and $B_1|B_1|^2$ in the cubic terms and results in the normal form obtained by Dias & Bridges (1994):

$$\left(\omega^2 - \varrho(1+b)\right) A_1 - 2\varrho A_1 \left[\left(\alpha_{11} + \beta_{11} + \frac{(1+b)^2}{4(1-2b)}\varrho^2\right)|A_1|^2 + (\alpha_{11} - \beta_{11})|B_1|^2\right] = 0,$$

$$\left(\omega^2 - \varrho(1+b)\right) B_1 - 2\varrho B_1 \left[(\alpha_{11} - \beta_{11})|A_1|^2 + \left(\alpha_{11} + \beta_{11} + \frac{(1+b)^2}{4(1-2b)}\varrho^2\right)|B_1|^2\right] = 0.$$

The quadratic terms have disappeared. The coefficients α_{11} and β_{11} are given in Appendix B. It can be shown that there are two types of solutions: travelling waves (*TW*s), characterized by A_1 or B_1 equal to zero, and standing waves (*SW*s), characterized by $|A_1| = |B_1|$, unless

$$2\beta_{11} + \frac{(1+b)^2}{4(1-2b)} = 0. \tag{2.19}$$

If the last condition is satisfied, both equations become identical and higher-order terms are needed (see Dias & Bridges 1994 for a detailed study of this degeneracy).

(*b*) *Reduction for* (1,2)*-waves*

This case, which corresponds to $\omega_0^2 = \varrho(1+b)$ and $2\omega_0^2 = \varrho(1+4b)$ being satisfied simultaneously, occurs when $b = \frac{1}{2}$. The coefficients of the fundamental mode and of the second harmonic are of the same order, which explains the terminology (1,2)-wave. If the normal form is truncated so that only the linear and quadratic terms are retained, one obtains

$$\begin{aligned}
\left(\omega^2 - \tfrac{3}{2}\varrho\right) A_1 - \varrho\omega^2 \overline{A_1} A_2 &= 0,\\
\left(\omega^2 - \tfrac{3}{2}\varrho\right) B_1 - \varrho\omega^2 \overline{B_1} B_2 &= 0,\\
\left(2\omega^2 - 3\varrho\right) A_2 - \tfrac{1}{2}\varrho\omega^2 A_1^2 &= 0,\\
\left(2\omega^2 - 3\varrho\right) B_2 - \tfrac{1}{2}\varrho\omega^2 B_1^2 &= 0.
\end{aligned}$$

The equations can be combined to give

$$\begin{aligned}
|A_1| &= 2|A_2|, \qquad & \sin(\varphi_2^a - 2\varphi_1^a) &= 0,\\
|B_1| &= 2|B_2|, \qquad & \sin(\varphi_2^b - 2\varphi_1^b) &= 0.
\end{aligned}$$

The effects of the cubic terms will be studied in the next sections.

(*c*) *Reduction for 2-waves*

This case corresponds to $2\omega_0^2 = \varrho(1+4b)$ while $\omega_0^2 \neq \varrho(1+b)$. The coefficients of the fundamental mode are zero, which explains the terminology 2-wave. The third and fourth equations of the normal form become

$$\left(2\omega^2 - \varrho(1+4b)\right) A_2 - 2\varrho A_2 \left[(\alpha_{22} + \beta_{22})|A_2|^2 + (\alpha_{22} - \beta_{22})|B_2|^2\right] = 0,$$

$$\left(2\omega^2 - \varrho(1+4b)\right) B_2 - 2\varrho B_2 \left[(\alpha_{22} - \beta_{22})|A_2|^2 + (\alpha_{22} + \beta_{22})|B_2|^2\right] = 0,$$

where the coefficients α_{22} and β_{22} are given in Appendix B. The above equations are in fact equivalent to the equations for the 1-waves with the scaling $\omega \to \frac{1}{2}\omega$, $k \to \frac{1}{2}k$ and as a consequence $b \to \frac{1}{4}b$. The degeneracy condition (2.19) simply becomes $\beta_{22} = 0$.

A 1-wave can become a (1,2)-wave and then a 2-wave in a continuous fashion. This phenomenon was well-described by Chen & Saffman (1979) who associated it with a bifurcation phenomenon in which a wave can double its wavelength. If cubic terms are neglected in (2.18), the normal form becomes

$$\begin{aligned}
\left(\omega^2 - \varrho(1+b)\right) a_1 &= \pm\varrho\omega^2 a_1 a_2, \\
\left(\omega^2 - \varrho(1+b)\right) b_1 &= \pm\varrho\omega^2 b_1 b_2, \\
\left(2\omega^2 - \varrho(1+4b)\right) a_2 &= \pm\tfrac{1}{2}\varrho\omega^2 a_1^2, \\
\left(2\omega^2 - \varrho(1+4b)\right) b_2 &= \pm\tfrac{1}{2}\varrho\omega^2 b_1^2.
\end{aligned}$$

Note that Nayfeh & Saric (1972) obtained a similar system for interfacial travelling waves, i.e. when either a_1 or b_1 is zero (see their equations 5.11 and 5.12). Eliminating ω^2 yields

$$\pm\tfrac{1}{2}\varrho(1+b)a_1^2 = (1-2b)a_2 \pm \varrho(1+4b)a_2^2 \qquad (\text{if } a_1 a_2 \neq 0), \tag{2.20}$$

$$\pm\tfrac{1}{2}\varrho(1+b)b_1^2 = (1-2b)b_2 \pm \varrho(1+4b)b_2^2 \qquad (\text{if } b_1 b_2 \neq 0). \tag{2.21}$$

Let us consider for example the case of a travelling wave with $b_1 = b_2 = 0$ and the plus signs in (2.20). If b is much smaller than $\frac{1}{2}$, a_2 is of the order of a_1^2 and the wave is a 1-wave. As b approaches $\frac{1}{2}$, the term in a_2 becomes small and a_2 is of the order of a_1. A dip appears in the crest and the wave becomes a (1,2)-wave. As b increases even more, the dip becomes larger. The right-hand side of (2.20) eventually becomes equal to zero and the wave becomes a 2-wave. If the minus signs are chosen, the same behaviour occurs, except that one starts with values of b much larger than $\frac{1}{2}$ and then lets b decrease.

In the following sections we study all solutions to the normal form (2.18). Bridges (1990) gave a classification of all solutions to normal forms for Hamiltonian systems with a mode interaction in the presence of the same symmetries as in the interfacial wave problem. In the particular case of the 1:2 resonance, Bridges found seven types of periodic solutions: three types of 2-waves (*TW*, *SW* and a degenerate wave when (2.19) is satisfied), three types of (1,2)-waves (one *TW* and two *SW*s), and mixed waves (*MW*s) in which either a_1 or b_1 is zero, the other three amplitudes being non-zero. The two types of (1,2)-*SW*s lie in fact on the same group orbit, so there is only one type of (1,2)-*SW*s to consider. Periodic 2-waves have been studied by Dias & Bridges (1994). The degenerate wave does not occur in the interfacial wave problem in the presence of the 1:2 resonance, because the degeneracy condition is never satisfied for b in a neighbourhood of $\frac{1}{2}$. Therefore, the study presented next focuses on three types of space- and time-periodic waves: (1,2)-*TW*s, (1,2)-*SW*s and *MW*s.

3. Analysis of the normal form for travelling waves

In this section, the normal form (2.18) derived in § 2 is analysed for travelling waves. There are two types of *TW*s: TW^+, travelling from left to right and characterized by $B_1 = B_2 = 0$, and TW^-, travelling from right to left and characterized by $A_1 = A_2 = 0$. Without loss of generality, the analysis is restricted to TW^+, the analysis for TW^- being similar. The normal form, truncated at order three, reduces to two

equations

$$\left(\omega^2 - \varrho(1+b)\right) a_1 - \varrho\omega^2 a_1 a_2 - 2\varrho a_1 \left[(\alpha_{11}+\beta_{11})a_1^2 + (\alpha_{12}+\beta_{12})a_2^2\right] = 0, \quad (3.1)$$

$$\left(2\omega^2 - \varrho(1+4b)\right) a_2 - \tfrac{1}{2}\varrho\omega^2 a_1^2 - 2\varrho a_2 \left[(\alpha_{12}+\beta_{12})a_1^2 + (\alpha_{22}+\beta_{22})a_2^2\right] = 0. \quad (3.2)$$

Note that the $\mp$ sign in front of the quadratic terms in (2.18) has been replaced by a minus sign by allowing a_2 to take negative values. Following a classification that is commonly used, we will refer to waves with $a_1 = 0$ as 2-waves, to (1,2)-waves with $a_2 > 0$ as *g-like* waves (*g* stands for gravity) and to (1,2)-waves with $a_2 < 0$ as *c-like* waves (*c* stands for capillary). The above equations agree with (3.9)–(3.10) in Bontozoglou & Hanratty (1990) (with no shear velocity between the layers). The energy of the wave is defined as $E = E_1 + 2E_2 = a_1^2 + 2a_2^2$, where E_1 and E_2 are defined in (2.12). Note that strictly speaking E is not the energy of the wave. The 'real' energy is given by $\mathscr{H}$ (2.17). For the analysis, E is a simpler parameter to use. However, whenever comparison is made with numerical values of the energy, it is of course $\mathscr{H}$ which must be used. A detailed analysis of the solutions to (3.1)–(3.2) is provided below. The corresponding system for water waves ($\varrho = 1$) has been studied rigorously by Jones & Toland (1986). They show that at exact resonance ($b = \frac{1}{2}$) there are three solutions bifurcating from the trivial solution, one 2-wave and two (1,2)-waves, whereas near resonance there are two solutions bifurcating from the trivial solution, one 2-wave and one (1,2)-wave, and one (1,2)-wave coming from a secondary bifurcation point on the 2-wave branch. This local result also holds for interfacial waves, but we show in this section that the cubic terms can modify significantly the structure of the solutions, especially for small values of ϱ.

Solutions for ω, a_1, a_2 are found either by specifying b and ϱ and using E as parameter, or by specifying ϱ and E and using b as parameter. In order to find (1,2)-waves, (3.1) can be divided by a_1. For 2-waves, the system reduces to the single equation

$$2\omega^2 - \varrho(1+4b) - 2\varrho(\alpha_{22}+\beta_{22})a_2^2 = 0. \quad (3.3)$$

It is easy to see that a bifurcation from a 2-wave to a (1,2)-wave will occur if the system

$$\omega^2 - \varrho(1+b) - \varrho\omega^2 a_2 - 2\varrho(\alpha_{12}+\beta_{12})a_2^2 = 0, \quad (3.4)$$

$$2\omega^2 - \varrho(1+4b) - 2\varrho(\alpha_{22}+\beta_{22})a_2^2 = 0, \quad (3.5)$$

has a non-trivial solution for given values of b and ϱ.

3.1. *Analysis at resonance*

In this subsection, b is equal to $\frac{1}{2}$. If cubic terms are neglected in (3.1)–(3.2), there are two solutions for given values of ϱ and E, a *g-like* wave and a *c-like* wave. However, if cubic terms are added, there might be three (1,2)-waves for particular values of the energy (in addition, of course, to the unique 2-wave solution). Two of the three are *g-like* waves, while the other is a *c-like* wave. The additional solution bifurcates from a 2-wave at a critical value of the energy which depends on ϱ. The bifurcation point is a solution to (3.4)–(3.5). This bifurcated wave, which is a *g-like* wave, will be henceforth referred to as a *g-like* II wave, while the *g-like* wave which bifurcates from the trivial solution will be called *g-like* I wave. A plot of the critical value of the energy versus ϱ is shown in figure 1. The validity of the normal form being restricted to small values of the energy, we can expect this bifurcation to occur at least for small values of ϱ. In §4, we confirm numerically that this bifurcation exists for sufficiently small values of ϱ. The numerical values for the critical energy have been added in

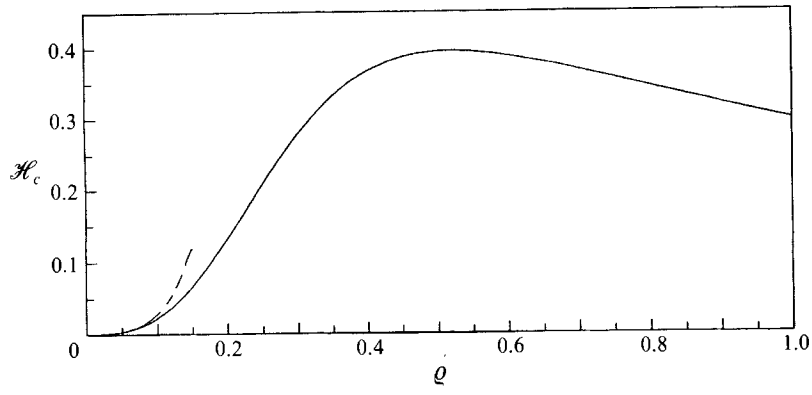

FIGURE 1. Path along which a (1,2)-*TW*, 2-*TW* bifurcation occurs at exact resonance (solid line: analytical results, broken line: numerical results).

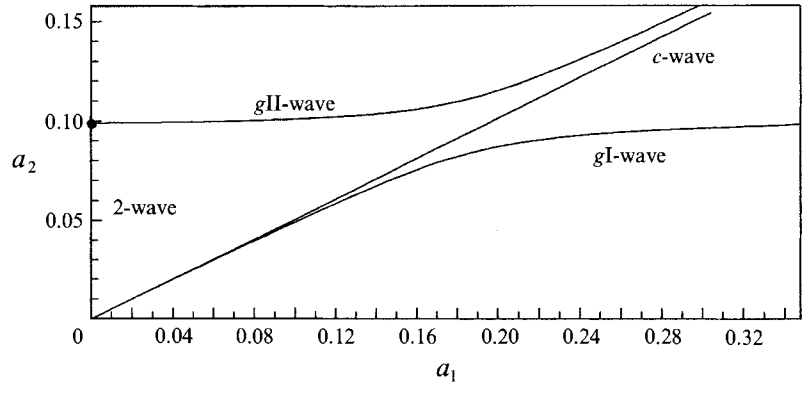

FIGURE 2. The four branches of *TW*s at exact resonance ($\varrho = 0.05$).

figure 1 for comparison. This bifurcation, which does not occur in the water-wave case, leads to a different behaviour of the solutions to (3.1)–(3.2). Therefore, from now on, the analysis will be focused on small values of ϱ. The results presented below in this section correspond to $\varrho = 0.05$. Figure 2 shows a plot of the amplitude a_2 versus the amplitude a_1 with the energy E as parameter along the four branches of travelling waves: *g-like* I, *g-like* II, *c-like* and 2-wave. Figure 5(*b*) shows the three branches of (1,2)-waves in addition to the branch of 2-waves in the (ω, E)-plane. For *TW*s, ω represents the dimensionless phase velocity of the wave. As explained above, the branch of *g-like* II waves bifurcates from the branch of 2-waves at a critical value of the energy. The other three branches bifurcate from the trivial solution. Note that the two branches of *g-like* waves are very close to each other.

3.2. *Analysis near resonance*

In this subsection, (3.1)–(3.2) are solved for b in a neighbourhood of $\frac{1}{2}$. First, the value of the energy E is fixed and b is used as parameter. Then the value of b is fixed and the energy E is used as parameter. The analysis for a fixed value of the energy clearly shows the origin of the third wave mentioned in the previous subsection. In figure 3, we have represented the branches of travelling waves in the (b, ω)-plane for

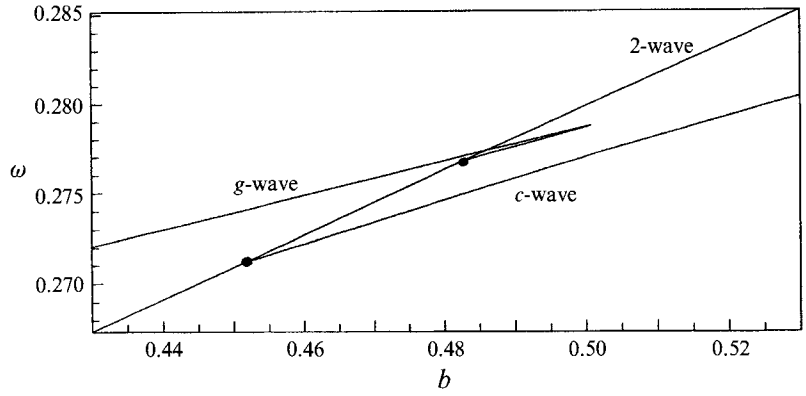

FIGURE 3. Branches of *TW*s for an energy $E = 0.088$ near resonance. The value of ϱ is 0.05. Both branches of (1,2)-waves end on the 2-wave branch, but there is a turning point on the branch of *g-like* waves. The coordinates of the bifurcation points (filled circles) are (0.45171,0.27122) and (0.48271,0.27675). The coordinates of the turning point are (0.50074,0.27875).

$E = 0.088$. As for the water-wave case, the branch of *c-like* waves bifurcates from the branch of 2-waves at a value of b smaller than $\frac{1}{2}$ (see for example figure 2 in Reeder & Shinbrot 1981*a*). The interesting feature of the plot is the behaviour of the branch of *g-like* waves: as opposed to the water-wave case where the branch of *g-like* waves bifurcates from the 2-wave branch at a value of b larger than $\frac{1}{2}$ (see again figure 2 in Reeder & Shinbrot 1981*a*), the branch of *g-like* waves bifurcates at a value of b smaller than $\frac{1}{2}$. The branch of *g-like* waves exhibits a turning point of very large curvature at a value of b larger than $\frac{1}{2}$. The presence of the turning point clearly explains the existence of the *g-like* II wave described in §3.1: the *g-like* II waves lie on the lower part of the *g-like* branch. The importance of turning points was recently emphasized by Aston (1993) in his study of mode interactions for capillary–gravity waves. However, he studied rigorously paths of turning points originating from the resonance on the trivial solution, while we are concerned here with a path of turning points which originates at a non-zero value of the energy. Moreover, our calculations are purely formal. The path of turning points with E as parameter can be obtained by adding to (3.1)–(3.2) the extra condition that the determinant of the Jacobian of these two equations be equal to zero. Figure 4 shows the path of turning points in the (b, ω)-plane. The path starts at $(b, \omega) = (0.50164, 0.27476)$ for an energy $E = 0.008767$. For $0.50029 < b < 0.50164$, there are two turning points. The consequence appears clearly in the bifurcation diagrams presented below. Figure 4 also shows the path of bifurcation points obtained by solving (3.4)–(3.5) and indicates the type of the bifurcated (1,2)-*TW* (*g-like* or *c-like*). There is no bifurcation point for $b > 0.50185$.

The bifurcation diagrams of figure 5 show the branches of *TW*s in the (ω, E)-plane. The branch of 2-waves always bifurcates from the trivial solution at $\omega^2 = \varrho(\frac{1}{2} + 2b)$. For $b < \frac{1}{2}$, there is a primary branch of *g-like* I waves. For $b > \frac{1}{2}$, there is a primary branch of *c-like* waves. These waves bifurcate at $\omega^2 = \varrho(1+b)$. For $b > 0.50029$, there is a branch of *g-like* waves which is not (locally) connected to the trivial solution. For $0.5 < b < 0.50029$, there are two secondary branches of *g-like* waves, which do not intersect each other (at least locally). For $0.50029 < b < 0.50164$, these two branches are globally connected. For $b > 0.50164$, the globally connected branches disappear. This rich structure of bifurcations is hard to visualize on the figures because some of

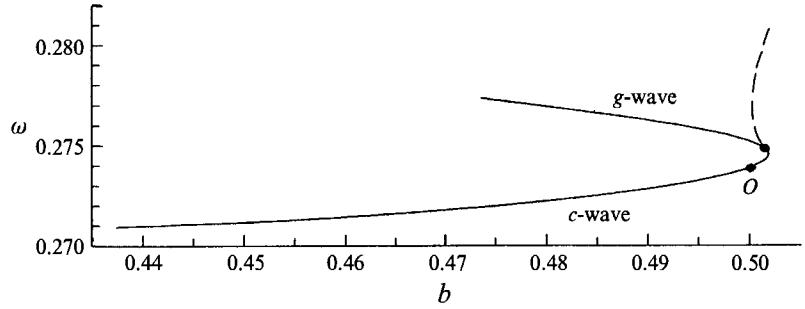

FIGURE 4. Paths of turning points (broken line) and of bifurcation points (solid lines) for the (1,2)-*TW*, 2-*TW* bifurcation for $\varrho = 0.05$. The type of the resulting (1,2)-*TW* is indicated. The parameter along the curves is the energy E. The curves only show points with $E < 0.12$. The point O, of coordinates (0.5,0.27386), corresponds to a zero energy. The path of turning points starts at (0.50164,0.27476). The path of bifurcation points turns at (0.50185,0.27453).

the branches lie on top of each other. That is why we have added figure 6, which shows the qualitative behaviour of the branches of *g-like* waves as b varies. In figure 6(a), the branches are locally disconnected. In figure 6(b), the branches intersect at one point, which is a degenerate turning point. In figure 6(c), there are two turning points, including one on the branch connected to the 2-wave branch. For $b > 0.50164$, the turning point on the lower branch has disappeared (see figure 6d). For $b > 0.50185$, the lower branch has disappeared (see figure 6e).

4. Numerical results for travelling waves

Numerical computations, based on the method that was used by Saffman & Yuen (1982) for computing finite-amplitude gravity interfacial waves in the presence of a current, were performed in order to confirm and extend the analytical results. Only a brief description of the scheme is given herein. For more details one can refer to the above-mentioned paper or Bontozoglou & Hanratty (1990), who modified the scheme to include capillarity.

For simplicity, the computations are performed in a frame of reference moving with the wave so that the flow is steady. For the sake of clarity, different symbols are used for the physical coordinates in each fluid: x, y for the lower fluid and x', y' for the upper fluid. The unit length and unit time are the same as in the analysis. Streamfunctions $\psi(x,y)$ and $\psi'(x',y')$ are introduced. Without loss of generality, ψ and ψ' are defined such that $\Psi = \Psi' = 0$, where $\Psi = \psi(x,\eta(x))$ and $\Psi' = \psi(x',\eta(x'))$. The physical coordinates below and above the interface are expressed as Fourier series (given below in truncated form) in ϕ, ψ and ϕ', ψ' respectively as follows:

$$x = \frac{\phi}{\omega} + \sum_{n=1}^{N} a_n \sin\left(n\frac{\phi}{\omega}\right) e^{n\psi/\omega}, \quad y = \frac{\psi}{\omega} + a_0 + \sum_{n=1}^{N} a_n \cos\left(n\frac{\phi}{\omega}\right) e^{n\psi/\omega}, \tag{4.1}$$

$$x' = \frac{\phi'}{\omega} + \sum_{n=1}^{N} a'_n \sin\left(n\frac{\phi'}{\omega}\right) e^{-n\psi'/\omega}, \quad y' = \frac{\psi'}{\omega} + a'_0 - \sum_{n=1}^{N} a'_n \cos\left(n\frac{\phi'}{\omega}\right) e^{-n\psi'/\omega}. \tag{4.2}$$

Note that the coefficients a_n and a'_n are different from the coefficients a_1 and a_2 used in the analysis. The total energy $\mathscr{H}$, the kinetic energy and the potential energy can be evaluated in terms of ω, ϱ and the coefficients in the Fourier series (see for example

Saffman & Yuen 1982), and are non-dimensionalized by an appropriate factor in order to allow comparison with the analysis. The fact that the two velocity potentials Φ and Φ' on the interface are not equal is treated numerically by introducing auxiliary variables s and ξ, defined by

$$s = \frac{1}{2}\left(\frac{\Phi'}{\omega} - \frac{\Phi}{\omega}\right), \qquad \xi = \frac{\Phi}{\omega} + s = \frac{\Phi'}{\omega} - s. \tag{4.3}$$

Next, the interface is discretized. Symmetry allows discretization over a half-period (from a crest to a trough for example) as follows:

$$\xi_i = \frac{(i-1)\pi}{N}, \quad i = 1, 2, \cdots, N+1. \tag{4.4}$$

Bernoulli's equation may be written in dimensionless form as

$$\tfrac{1}{2}(1+\varrho)|\boldsymbol{u}|^2 - \tfrac{1}{2}(1-\varrho)|\boldsymbol{u}'|^2 + 2\varrho\eta - 2\varrho b\frac{\eta_{xx}}{(1+\eta_x^2)^{\frac{3}{2}}} = \gamma. \tag{4.5}$$

The constant γ, which is equal to $\varrho\omega^2$, is kept in the algorithm as an unknown to be used at the end as a check on the accuracy of the results. Equation (4.5) provides a set of $N+1$ nonlinear equations to be satisfied at each ξ_i ($i = 1, ..., N+1$).

The fact that the curves described by (4.1)–(4.2) coincide at the interface requires that $x = x'$ and $y = y'$; that is, using (4.3),

$$\xi - s + \sum_{n=1}^{N} a_n \sin n(\xi - s) = \xi + s + \sum_{n=1}^{N} a'_n \sin n(\xi + s), \tag{4.6}$$

$$a_0 + \sum_{n=1}^{N} a_n \cos n(\xi - s) = a'_0 - \sum_{n=1}^{N} a'_n \cos n(\xi + s). \tag{4.7}$$

Equations (4.6)–(4.7), when satisfied at each ξ_i ($i = 1, ..., N+1$), provide another set of nonlinear equations. Since the auxiliary equations for the crest and trough,

$$s(0) = s(\pi) = 0,$$

result in (4.6) being satisfied identically at the endpoints, we obtain $2N$ equations from (4.6)–(4.7). This increases the total number of equations to $3N+1$ in $3N+3$ unknowns, namely a_0, a_1, ..., a_N, a'_0, a'_1, ..., a'_N, s_2, ..., s_N, γ and ω. Specifying the mean interfacial elevation (to be zero for example) and either the wave height h defined as $\eta(0) - \eta(\pi)$ (the drawback of this definition of height is clear since 2-waves then have a zero height!) or the total energy $\mathscr{H}$ provides the last two equations.

With ϱ, b and h (or $\mathscr{H}$) as parameters, the resulting system is solved by Newton's method. A sine wave may be used as an initial guess for small wave height h.

In all the computations presented below, forty mesh points ($N = 40$) were used, a number which was found sufficient to ensure accuracy for computing waves with small energy. For more details on the accuracy of the scheme, readers may refer to Saffman & Yuen (1982) or Bontozoglou & Hanratty (1990).

In order to compare numerical results to analytical results, the analytical wave height must be computed. For TW^+s, the elevation of the interface at second order is

$$\eta = \mathrm{Re}\left[A_1 e^{-i(\omega t - x)} + A_2 e^{-i(2\omega t - 2x)} + A_3 e^{-i(3\omega t - 3x)} + A_4 e^{-i(4\omega t - 4x)}\right].$$

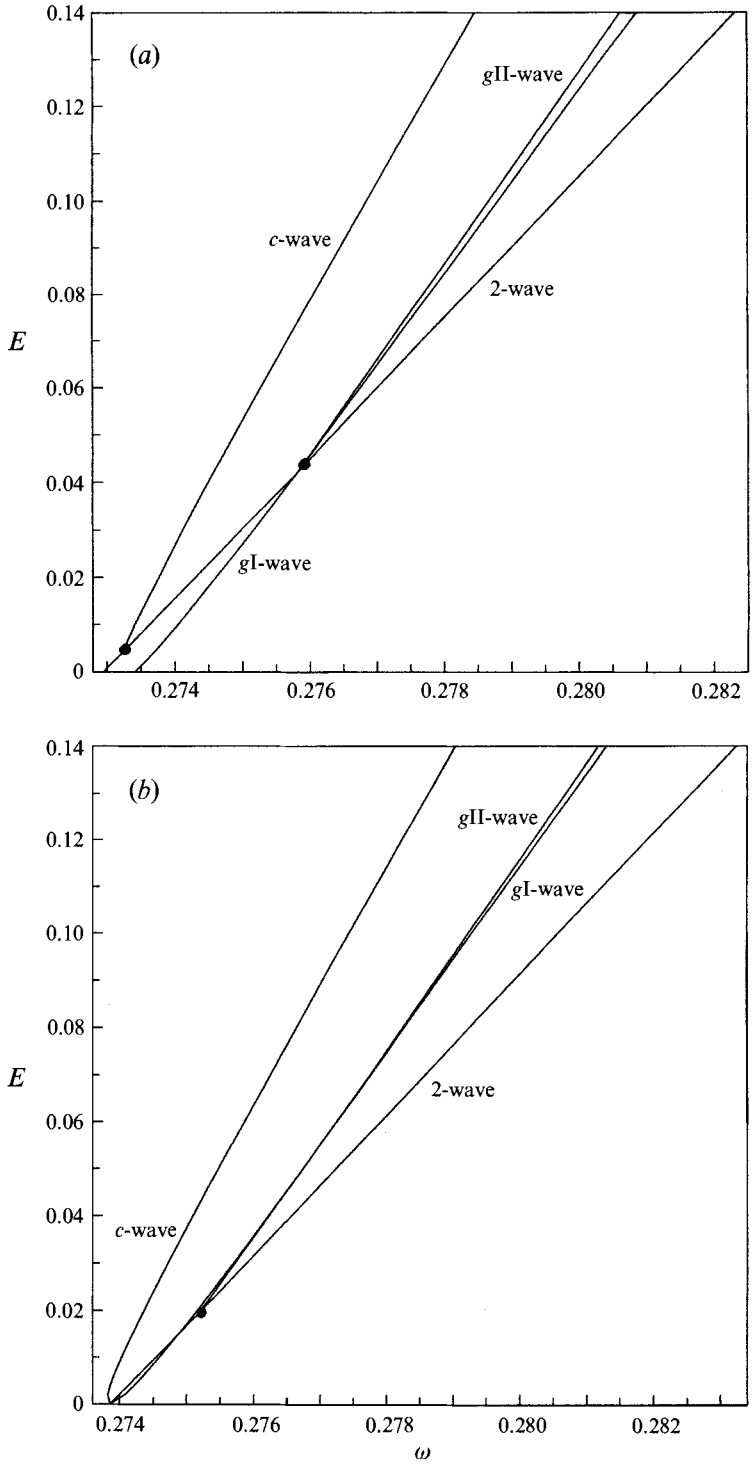

FIGURE 5 (a, b). For caption see facing page.

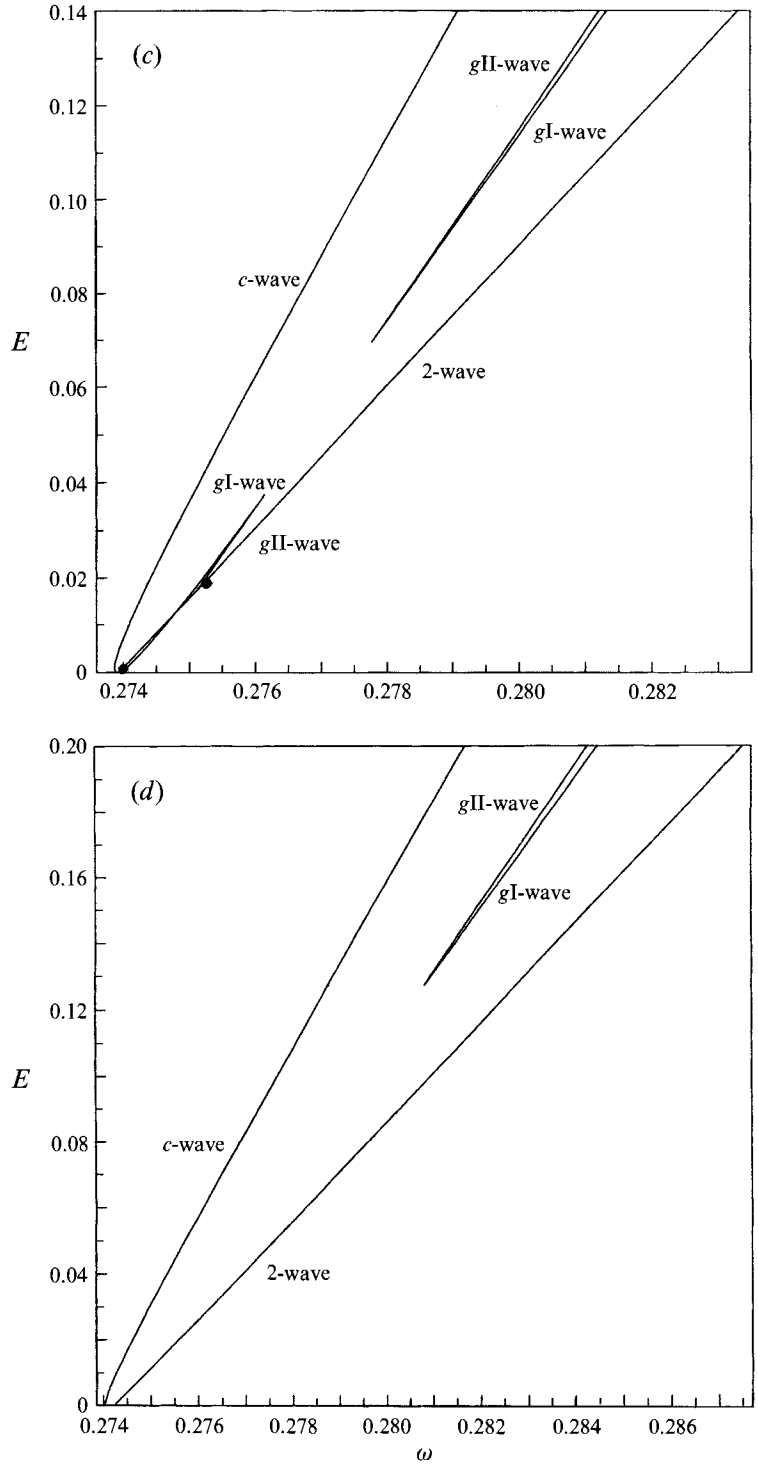

FIGURE 5. *TW* bifurcation diagrams for $\varrho = 0.05$ for (*a*) $b = 0.495$, (*b*) $b = 0.5$ (exact resonance), (*c*) $b = 0.5004$, (*d*) $b = 0.502$. The filled circles indicate bifurcation from a non-trivial solution.

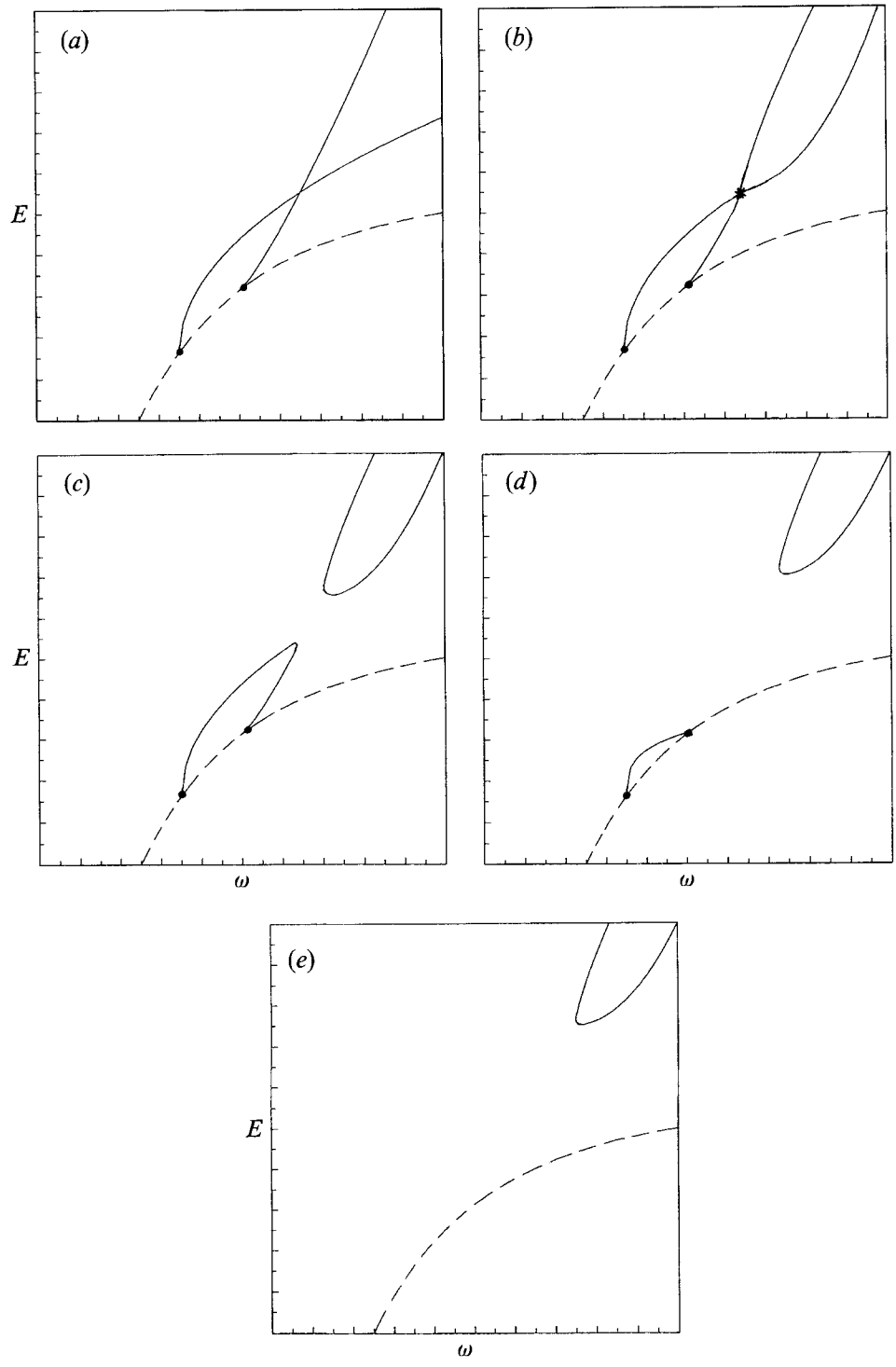

FIGURE 6. Qualitative description of the changes in the branches of *g-like TW*s (solid lines) for $\varrho = 0.05$ as b varies: (*a*) $0.5 < b < 0.50029$, (*b*) $b = 0.50029$ (the cross indicates that the branches intersect), (*c*) $0.50029 < b < 0.50164$, (*d*) $0.50164 < b < 0.50185$, (*e*) $b > 0.50185$. The broken line is the branch of 2-*TW*s. The filled circles indicate bifurcation from a non-trivial solution.

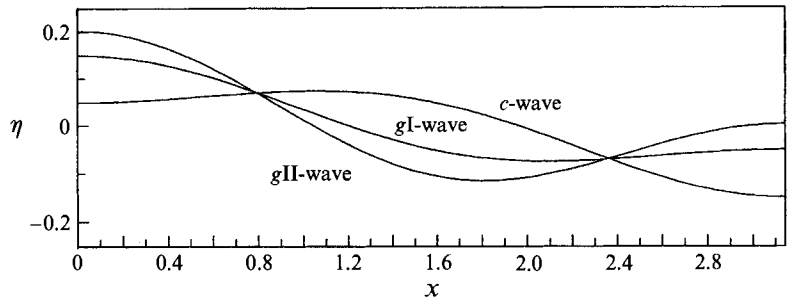

FIGURE 7. Numerical profiles of the three (1,2)-*TW*s for $h = 0.2$, $b = 0.5$, $\varrho = 0.05$. The values for the energy $\mathscr{H}$ and wave speed ω are 0.004667 and 0.275780 for the *g-like* II wave, 0.002247 and 0.274882 for the *g-like* I wave, 0.002216 and 0.274169 for the *c-like* wave.

In the process of constructing $\mathscr{L}$, one can find that

$$A_3 = \frac{\varrho(1+b)}{1-3b} A_1 A_2 .$$

The wave height is then found to be

$$h = 2\left(a_1 + \frac{\varrho(1+b)}{1-3b} a_1 a_2\right),$$

with again the convention that a_2 takes negative values for *c-like* waves.

4.1. *Results at exact resonance*

The analysis of the normal form for *TW*s done in § 3 suggested that at resonance ($b = \frac{1}{2}$) a third wave (of *g-like* type) exists in addition to the two well-known Wilton's ripples and that it bifurcates from a 2-wave at a critical value of the energy. For example, for a density parameter $\varrho = 0.05$, the weakly nonlinear analysis predicted that $\mathscr{H}_c = 0.002934$ (see figure 1). By choosing an energy value above the predicted one for $\mathscr{H}_c$ and using an initial guess based on the weakly nonlinear analysis, we indeed obtained a *g-like* II wave (recall the terminology introduced in § 3 in order to distinguish a *g-like* II wave from a *g-like* I wave, the usual *g-like* Wilton's ripple). In figure 7, we present these two waves along with the *c-like* wave, for a fixed wave height $h = 0.20$. Figures 8–10 show profiles of each of the three types of waves for various wave heights. Figure 8 shows profiles of *c-like* waves. Comparing with results obtained for *c-like* water waves by Hogan (1981), one can observe that the two behaviours are quite similar. For the *g-like* I type, however, the behaviour is different as the wave height increases: the interaction between the fundamental mode and the second harmonic weakens and the wave becomes a 1-wave. Recall that we say that a (1,2)-wave becomes a 1-wave when the dip in its profile disappears. Figure 9 shows profiles of this type. Profiles of *g-like* II waves are shown in figure 10. Note that the energy corresponding to the 2-wave is 0.003089, which agrees well with the prediction of the analysis (0.002934).

More information on each type of wave may be obtained by looking at table 1, which provides comparisons between numerical and analytical values for the wave speed ω, the kinetic energy and the potential energy, with waveheight as parameter. Figure 11 shows the branches of *TW*s in the (h, ω)-plane.

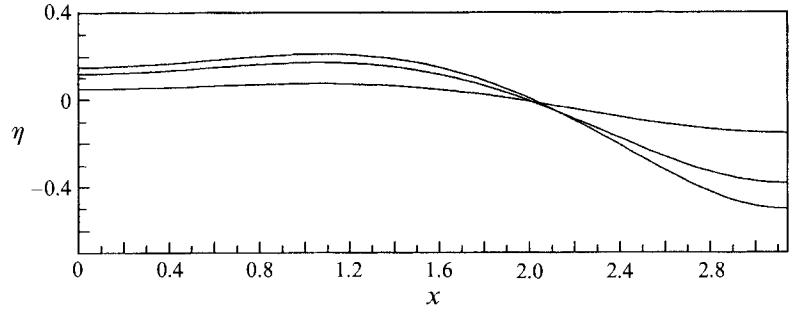

FIGURE 8. Numerical profiles of *c-like TW*s for $b = 0.5$, $\varrho = 0.05$ and $h = 0.2, 0.5, 0.65$.

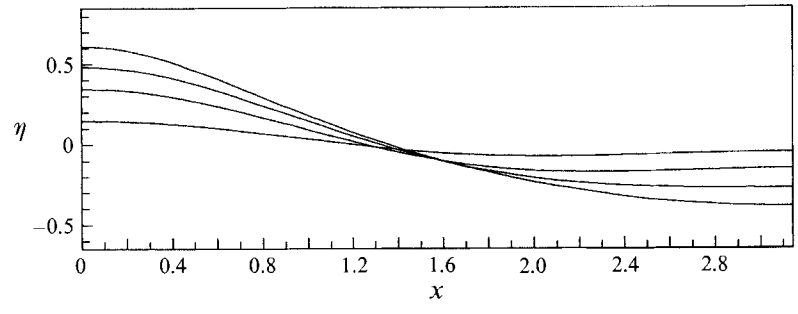

FIGURE 9. Numerical profiles of *g-like* I *TW*s for $b = 0.5$, $\varrho = 0.05$ and $h = 0.2, 0.5, 0.76, 1$.

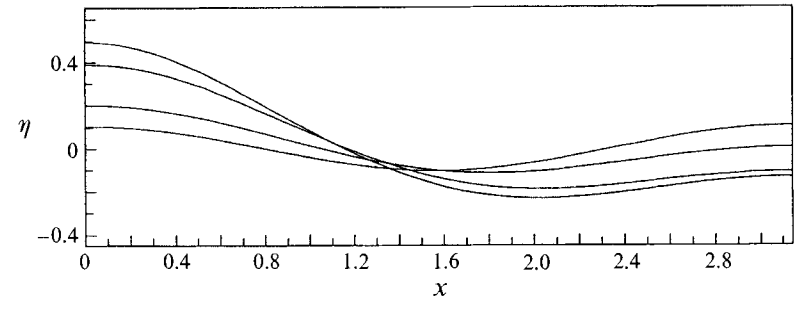

FIGURE 10. Numerical profiles of *g-like* II *TW*s for $b = 0.5$, $\varrho = 0.05$ and $h = 0, 0.2, 0.5, 0.63$.

4.2. *Results near resonance*

The next step is to confirm numerically the conjectures of § 3 near resonance. Again, the computations are performed for $\varrho = 0.05$. As can be seen in figure 1, the critical value of the energy for the bifurcation from a 2-wave to a *g-like* (1,2)-wave to occur increases rapidly with ϱ. As a result, even a slight increase in ϱ requires a large increase in the steepness of the bifurcating 2-wave. This is demonstrated in table 2 where the amplitude of the bifurcating 2-wave is tabulated against ϱ. With the present numerical scheme, we were not able to detect the bifurcation for values of ϱ larger than 0.15 because of the large steepness of the wave.

In order to study numerically the branching behaviour in a neighbourhood of

h	ω (N)	ω (A)	K (N)	K (A)	V (N)	V (A)
0.00	0.275249	0.275193	0.001548	0.001470	0.001541	0.001464
0.10	0.275381	0.275333	0.001745	0.001674	0.001735	0.001666
0.20	0.275780	0.275757	0.002342	0.002295	0.002325	0.002280
0.30	0.276460	0.276497	0.003373	0.003384	0.003345	0.003353
0.40	0.277505	0.277672	0.005011	0.005133	0.004950	0.005066
0.50	0.278953	0.279375	0.007417	0.007722	0.007291	0.007574
0.60	0.280594	0.281520	0.010401	0.011056	0.010170	0.010758
0.63	0.281108	0.282242	0.011498	0.012192	0.011227	0.011832
			g-like II wave			
0.00	0.273861	0.273861	0	0	0	0
0.10	0.274203	0.274203	0.000281	0.000282	0.000281	0.000282
0.20	0.274882	0.274883	0.001126	0.001128	0.001121	0.001124
0.30	0.275856	0.275877	0.002489	0.002503	0.002472	0.002486
0.40	0.276983	0.277067	0.004181	0.004233	0.004139	0.004186
0.50	0.278132	0.278364	0.005989	0.006160	0.005903	0.006064
0.60	0.279372	0.279854	0.008018	0.008405	0.007871	0.008229
0.65	0.280032	0.280687	0.009133	0.009672	0.008944	0.009441
0.75	0.281407	0.282537	0.011552	0.012517	0.011264	0.012135
1.00	0.284849	0.288231	0.018606	0.021550	0.017842	0.020449
			g-like I wave			
0.00	0.273861	0.273861	0	0	0	0
0.10	0.273857	0.273859	0.000279	0.000279	0.000279	0.000280
0.20	0.274169	0.274190	0.001109	0.001112	0.001107	0.001111
0.30	0.274756	0.274845	0.002465	0.002487	0.002457	0.002476
0.40	0.275552	0.275815	0.004318	0.004392	0.004290	0.004356
0.50	0.276465	0.277088	0.006617	0.006815	0.006552	0.006727
0.60	0.277372	0.278653	0.009290	0.009748	0.009173	0.009563
0.65	0.277856	0.279541	0.010737	0.011401	0.010590	0.011146
			c-like wave			

TABLE 1. Wave speed, kinetic energy and potential energy as functions of wave height for the three types of (1,2)-*TW*s, at exact resonance and for $\varrho = 0.05$. Comparison between numerical (N) and analytical (A) results.

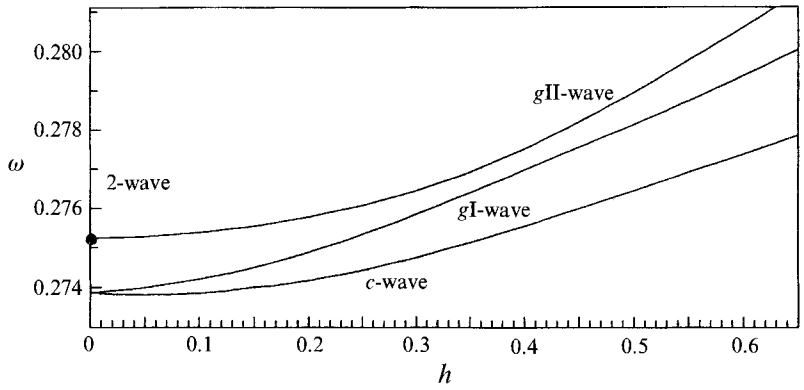

FIGURE 11. Numerical branches of *TW*s at exact resonance for $\varrho = 0.05$.

ϱ	N	A
0.050000	0.1018	0.0990
0.058201	0.1192	0.1148
0.069519	0.1437	0.1363
0.081081	0.1697	0.1579
0.092896	0.1977	0.1793
0.104972	0.2281	0.2005
0.111111	0.2445	0.2110
0.117318	0.2621	0.2214
0.129944	0.30	0.2419
0.142857	0.34	0.2618

TABLE 2. Amplitude of the bifurcating 2-wave as a function of ϱ at exact resonance. Comparison between analytical (A) and numerical (N) results.

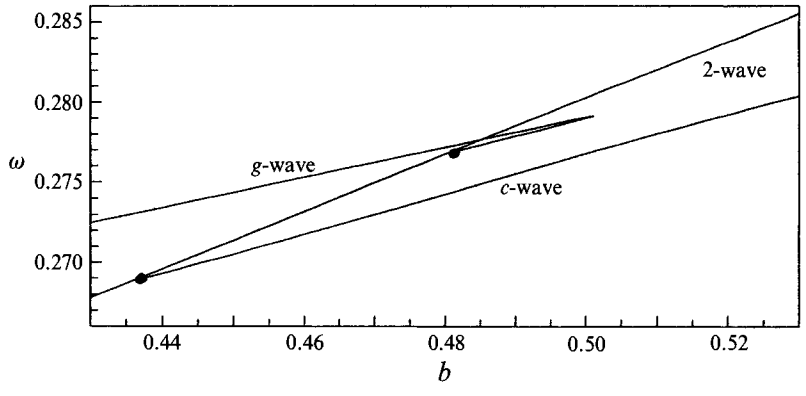

FIGURE 12. Numerical branches of *TW*s for $\varrho = 0.05$ and an energy $\mathscr{H} = 0.014847$ near resonance.

$b = \frac{1}{2}$, we chose $\mathscr{H} = 0.014847$ and studied the variation of the wave speed ω with b for each branch of *TW*s. The results are presented in figure 12. Note that the curves are not straight lines! The transition from a 1-wave to a (1,2)-wave (the *g-like* I type) occurs at (0.496, 0.27867) and the transition to a (1,2)-wave of *g-like* II type occurs at the turning point (0.50106, 0.27914). The *g-like* II wave becomes a 2-wave at (0.47999, 0.27676). The evolution of the *c-like* branch is quite similar to the water-wave case. The 1-wave becomes a (1,2)-wave of *c-like* type at (0.527, 0.28003) and a 2-wave at (0.437, 0.26905). Profiles of the different types of *TW*s are shown in figure 13 for various values of b.

The conclusion of this section is that the analytical results for travelling waves have been confirmed numerically. More numerical work is needed however to follow the branches of *TW*s as their amplitude becomes large. Moreover, as *TW*s with small energy were computed numerically, some bifurcations were detected, which were not predicted by the weakly nonlinear analysis. These bifurcations are associated with higher-order terms that were neglected in the Fourier series expansions (truncated at $N = 4$ in the present analysis).

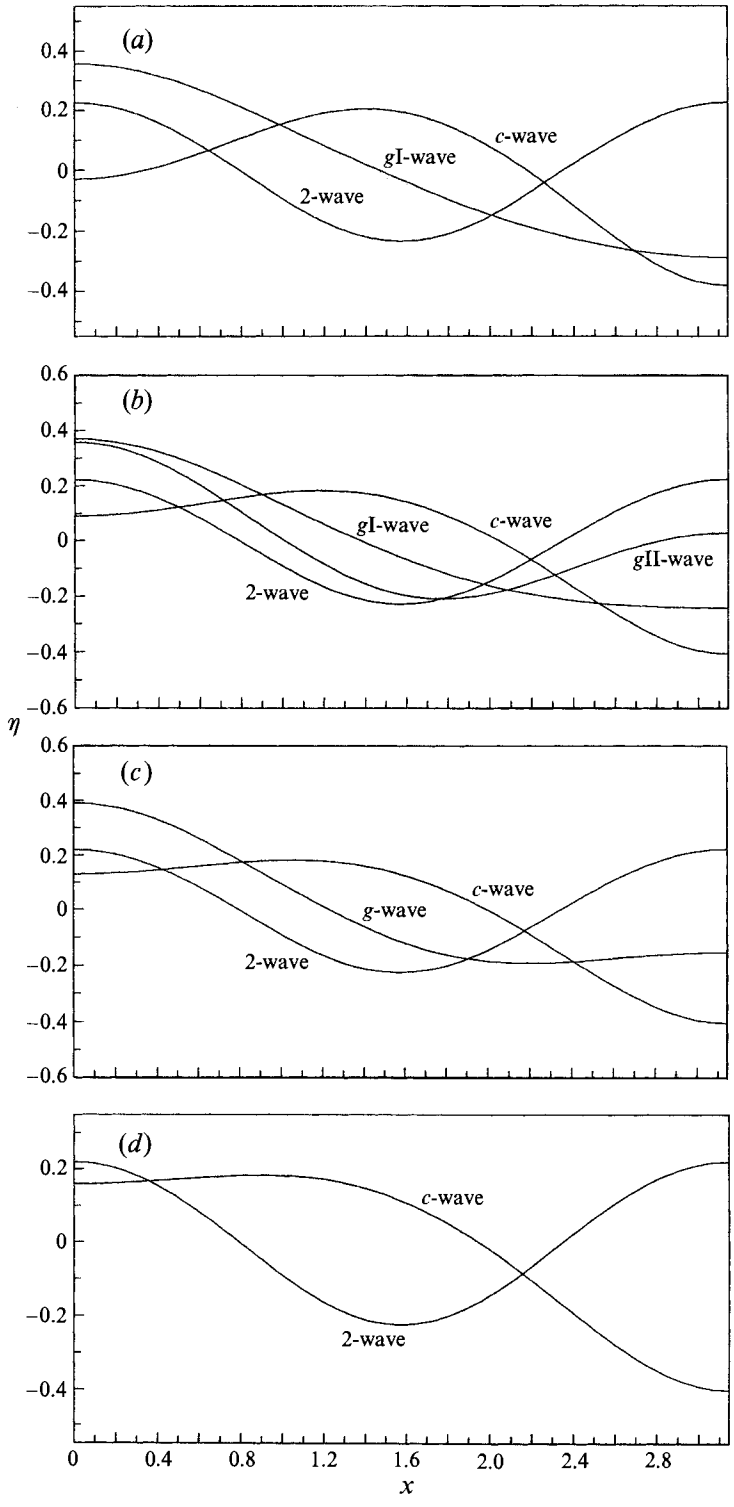

FIGURE 13. Numerical profiles of *TW*s with the same energy $\mathscr{H} = 0.014847$ for (*a*) $b = 0.46$, (*b*) $b = 0.49$, (*c*) $b = 0.50106$, (*d*) $b = 0.51$.

5. Analysis of the normal form for standing waves

Standing waves are characterized by $|A_1| = |B_1|$ and $|A_2| = |B_2|$. The normal form (2.18), truncated at order three, reduces to two equations

$$\left(\omega^2 - \varrho(1+b)\right) a_1 - \varrho\omega^2 a_1 a_2 - 4\varrho a_1(\alpha_{11}a_1^2 + \alpha_{12}a_2^2) = 0, \tag{5.1}$$

$$\left(2\omega^2 - \varrho(1+4b)\right) a_2 - \tfrac{1}{2}\varrho\omega^2 a_1^2 - 4\varrho a_2(\alpha_{12}a_1^2 + \alpha_{22}a_2^2) = 0. \tag{5.2}$$

Note that again the $\mp$ sign in front of the quadratic terms in (2.18) has been replaced by a minus sign by allowing a_2 to take negative values. Following the classification for *TW*s, we will refer to waves with $a_2 > 0$ as *g-like* waves and waves with $a_2 < 0$ as *c-like* waves. We define the energy of the wave as $E = E_1 + 2E_2 = 2a_1^2 + 4a_2^2$, where E_1 and E_2 are defined in (2.12). The local behaviour of the solutions is the same as for *TW*s. But again we show that the cubic terms can significantly change the branching behaviour. A detailed analysis of the solutions to (5.1)–(5.2) is provided below. Solutions for ω, a_1, a_2 are found either by specifying b and ϱ and using E as parameter, or by specifying ϱ and E and using b as parameter. In order to find (1,2)-waves, (5.1) can be divided by a_1. For 2-waves, the system reduces to the single equation

$$2\omega^2 - \varrho(1+4b) - 4\varrho\alpha_{22}a_2^2 = 0. \tag{5.3}$$

It is easy to see that a bifurcation from a 2-*SW* to a (1,2)-*SW* will occur if the system

$$\omega^2 - \varrho(1+b) - \varrho\omega^2 a_2 - 4\varrho\alpha_{12}a_2^2 = 0, \tag{5.4}$$

$$2\omega^2 - \varrho(1+4b) - 4\varrho\alpha_{22}a_2^2 = 0 \tag{5.5}$$

has a non-trivial solution for given values of b and ϱ. Standing Wilton's ripples have been studied by Vanden-Broeck (1984) analytically and numerically in the case of water waves ($\varrho = 1$).

5.1. *Analysis at resonance*

In this subsection, b is equal to $\frac{1}{2}$. If cubic terms are neglected in the system of equations (5.1)–(5.2), there are two (1,2)-*SW*s for given values of ϱ and E, a *g-like* wave and a *c-like* wave. However, if cubic terms are added, only one (1,2)-*SW* might be present for particular values of the energy (always in addition, of course, to the 2-wave solution corresponding to $a_1 = 0$). What happens is that the *c-like* wave becomes a 2-wave. The bifurcation point is a solution to (5.4)–(5.5). The critical energy $E_c(\varrho)$ at the bifurcation point is shown in figure 14. Bearing in mind that the system (5.1)–(5.2) is valid only for small-energy waves, we can predict that this bifurcation phenomenon is likely to occur for small values of ϱ. Again, we take $\varrho = 0.05$ in the analysis below. Figure 15 shows a plot of the amplitude a_2 versus the amplitude a_1 with the energy as parameter for the three branches of *SW*s. It is clearly demonstrated that the branch of *c-like* waves ends on the branch of 2-waves.

5.2. *Analysis near resonance*

In this subsection, (5.1)–(5.2) are solved for b in a neighbourhood of $\frac{1}{2}$. First the value of the energy is fixed and b is used as parameter. The resulting branches of standing waves are shown in figure 16. Since the chosen value for E is above the critical value at exact resonance, the branch of *c-like SW*s ends on the right of $b = \frac{1}{2}$. Figure 17 shows the path of bifurcation points obtained by solving (5.4)–(5.5) with the energy as parameter and indicates the type of the bifurcated (1,2)-*SW* (*g-like* or *c-like*). There is no bifurcation point for b less than 0.49953. No turning points have been found for

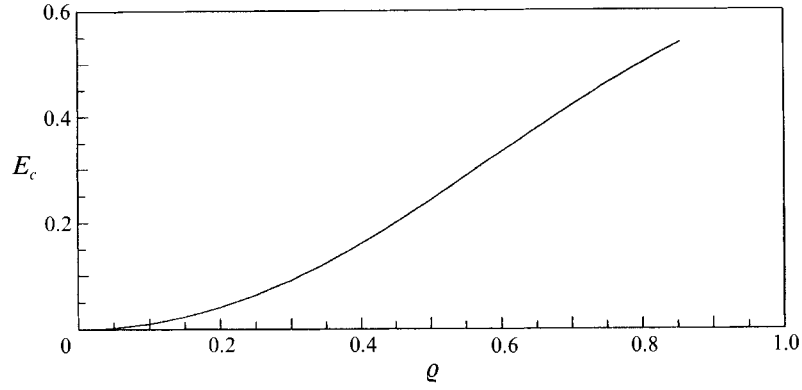

FIGURE 14. Path along which a (1,2)-*SW*, 2-*SW* bifurcation occurs at exact resonance.

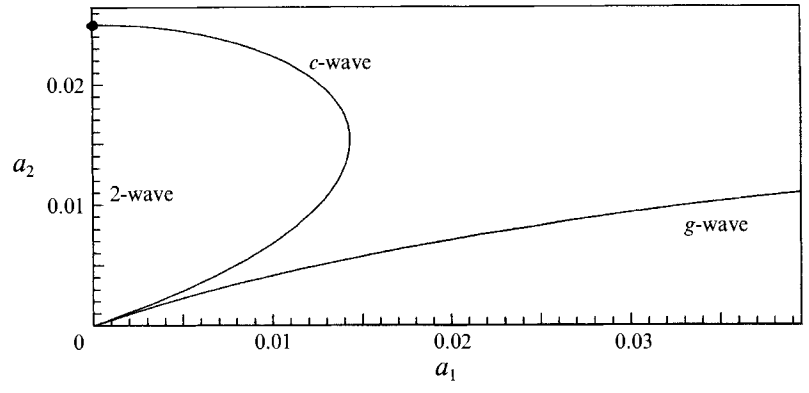

FIGURE 15. The three branches of *SW*s at exact resonance ($\varrho = 0.05$).

the branches of (1,2)-*SW*s. Bifurcation diagrams are shown in figure 18. The branch of 2-waves always bifurcates from the trivial solution at $\omega^2 = \varrho(\frac{1}{2} + 2b)$. For $b < \frac{1}{2}$, there is a primary branch of *g-like* waves. For $b > \frac{1}{2}$, there is a primary branch of *c-like* waves. These waves bifurcate at $\omega^2 = \varrho(1 + b)$. For $b < 0.49953$, there is no branch of *c-like* waves. For $0.49953 < b < 0.5$, there is a secondary branch of *c-like* waves which is globally connected to the branch of 2-waves. Note that it almost lies on top of the branch of 2-waves and is therefore hard to see in figure 18(*b*). For $b > \frac{1}{2}$, there is a secondary branch of *g-like* waves, which bifurcates from the branch of 2-waves.

The structure of all the branches of *SW*s described above has not been checked numerically yet. The numerical computation of *SW*s with surface tension is quite difficult and is still an area of active research. It would be of interest of course to confirm numerically the analytical results obtained in this section and to extend them to finite-amplitude waves.

6. Analysis of the normal form for mixed waves

These periodic waves, which are neither *TW*s nor *SW*s, are three-mode waves characterized by either $A_1 = 0$ (MW^+) or $B_1 = 0$ (MW^-). Since the analysis is similar

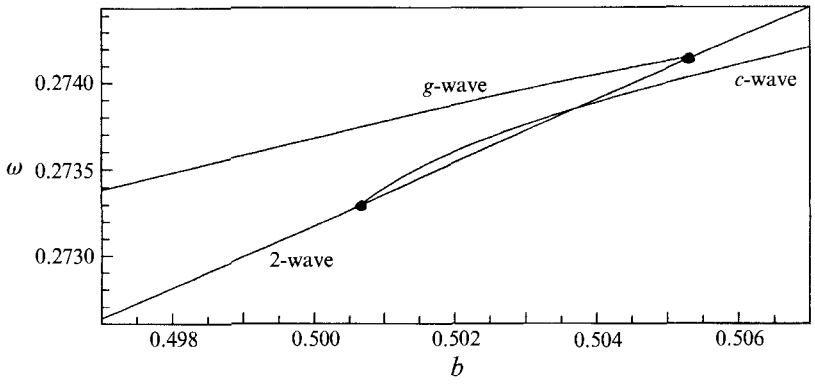

FIGURE 16. Branches of *SW*s for an energy $E = 0.004$ near resonance. The value of ϱ is 0.05. Both branches of (1,2)-waves end on the 2-wave branch, but the branch of *c-like* waves ends for a value of b larger than 0.5. The coordinates of the bifurcation points (filled circles) are (0.50063,0.27329) and (0.50539,0.27415).

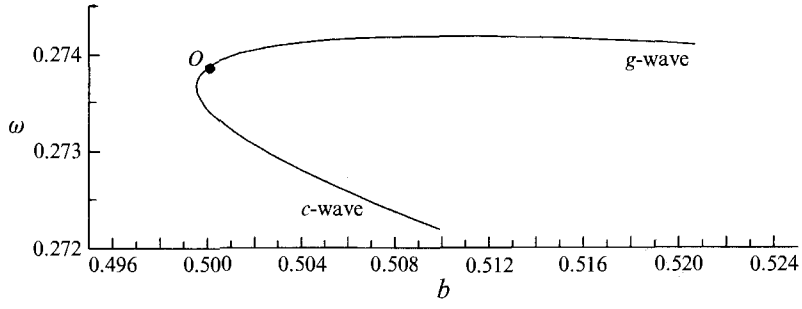

FIGURE 17. Paths of bifurcation points for the (1,2)-*SW*, 2-*SW* bifurcation for $\varrho = 0.05$. The type of the resulting (1,2)-*SW* is indicated. The parameter along the curves is the energy E. The point O, of coordinates (0.5,0.27386), corresponds to a zero energy. The curves only show points with $E < 0.02$. The path of bifurcation points turns at (0.49953,0.27367).

for both types, we concentrate on the case $B_1 = 0$ (and simply denote the mixed waves by *MW*). The normal form (2.18), truncated at order three, reduces to three equations since the second one is identically zero:

$$\omega^2 - \varrho(1+b) - \varrho\omega^2 a_2 - 2\varrho\left[(\alpha_{11}+\beta_{11})a_1^2 + \alpha_{12}E_2 - \beta_{12}M_2\right] = 0, \quad (6.1)$$

$$\left(2\omega^2 - \varrho(1+4b)\right)a_2 - \tfrac{1}{2}\varrho\omega^2 a_1^2 - 2\varrho a_2\left[(\alpha_{12}+\beta_{12})a_1^2 + \alpha_{22}E_2 - \beta_{22}M_2\right] = 0, \quad (6.2)$$

$$2\omega^2 - \varrho(1+4b) - 2\varrho\left[(\alpha_{12}-\beta_{12})a_1^2 + \alpha_{22}E_2 + \beta_{22}M_2\right] = 0. \quad (6.3)$$

The third equation has been divided by b_2, which is assumed to be non-zero. Again, allowing a_2 to take negative values has led to replacing the $\mp$ sign in front of the quadratic terms by a minus sign. Following the classification for *TW*s and *SW*s, waves with $a_2 > 0$ are called *g-like MW*s and waves with $a_2 < 0$ are called *c-like MW*s. Again the energy of the wave is $E = E_1 + 2E_2 = a_1^2 + 2(a_2^2 + b_2^2)$, where E_1 and E_2 are defined in (2.12). Solutions to (6.1)–(6.3) for ω, a_1, a_2 are found either by specifying b and ϱ and using E as parameter, or by specifying ϱ and E and using b as parameter. Several bifurcations can occur. The conditions for each one to occur are given below.

(*a*) *Bifurcation* (1,2)-*TW, MW*

This bifurcation occurs when the amplitude b_2 becomes zero. This is the case when

$$\omega^2 - \varrho(1+b) - \varrho\omega^2 a_2 - 2\varrho\left[(\alpha_{11}+\beta_{11})a_1^2 + (\alpha_{12}+\beta_{12})a_2^2\right] = 0, \quad (6.4)$$

$$\left(2\omega^2 - \varrho(1+4b)\right)a_2 - \tfrac{1}{2}\varrho\omega^2 a_1^2 - 2\varrho a_2\left[(\alpha_{12}+\beta_{12})a_1^2 + (\alpha_{22}+\beta_{22})a_2^2\right] = 0, \quad (6.5)$$

$$2\omega^2 - \varrho(1+4b) - 2\varrho\left[(\alpha_{12}-\beta_{12})a_1^2 + (\alpha_{22}-\beta_{22})a_2^2\right] = 0 \quad (6.6)$$

has a non-trivial solution for given values of b and ϱ. Note that this is a bifurcation from a (1,2)-TW^+ to a MW^-.

(*b*) *Bifurcation* 2-*SW, MW*

This bifurcation occurs when the amplitude a_1 becomes zero, with $a_2 b_2 \neq 0$. It follows that $a_2 = b_2$, unless the degeneracy condition $\beta_{22} = 0$ is satisfied, which is never the case near or at resonance. As a result, an MW becomes a 2-SW if

$$\omega^2 - \varrho(1+b) - \varrho\omega^2 a_2 - 4\varrho\alpha_{12}a_2^2 = 0, \quad (6.7)$$

$$2\omega^2 - \varrho(1+4b) - 4\varrho\alpha_{22}a_2^2 = 0 \quad (6.8)$$

has a non-trivial solution for given values of b and ϱ. Note that the conditions (6.7)–(6.8) are exactly the same as the conditions (5.4)–(5.5) for the bifurcation from a 2-SW to a (1,2)-SW to occur! Therefore a multiple bifurcation occurs at such points.

(*c*) *Bifurcation* 2-*TW, MW*

This bifurcation occurs when the amplitudes a_1 and a_2 or a_1 and b_2 become zero simultaneously. The case $(a_1, b_2) = (0,0)$ is not possible because equations (6.2)–(6.3) lead to $\beta_{22}a_2^2 = 0$, which implies that $a_2 = 0$ too. The case $(a_1, a_2) = (0,0)$ is possible and corresponds to the bifurcation from a 2-TW^- to an MW^-. It occurs if

$$\omega^2 - \varrho(1+b) - 2\varrho(\alpha_{12}-\beta_{12})b_2^2 = 0, \quad (6.9)$$

$$2\omega^2 - \varrho(1+4b) - 2\varrho(\alpha_{22}+\beta_{22})b_2^2 = 0 \quad (6.10)$$

has a non-trivial solution for given values of b and ϱ.

6.1. *Analysis at resonance*

In this subsection, b is equal to $\frac{1}{2}$. Results for $\varrho = 0.05$ and for $\varrho = 1$ (water waves) are presented below. Figure 19 shows plots of the three amplitudes a_1, a_2, b_2 as the energy varies, for $\varrho = 0.05$. The bifurcation points clearly appear on the plots. There is a primary branch of *g-like MWs* which bifurcates from the trivial solution. There is a branch of *c-like MWs*, not connected to the trivial solution, which bifurcates at one end from the branch of 2-SWs and at the other end from the branch of (1,2)-TWs. The same branches are shown in the (ω, E)-plane in figure 20(*a*): *c-like MWs* exist only for values of the energy between 0.00007 and 0.00250. Figure 20(*b*) shows the branches of mixed water waves: the bifurcation 2-SW, MW does not occur, at least for small values of the energy.

6.2. *Analysis near resonance*

In this subsection, equations (6.1)–(6.3) are solved for $\varrho = 0.05$ and for b in a neighbourhood of $\frac{1}{2}$. First, we look for possible bifurcations by solving the three systems (6.4)–(6.6), (6.7)–(6.8) and (6.9)–(6.10). The system (6.7)–(6.8) has been solved in § 5 and the path of bifurcation points is shown in figure 17. The bifurcation from a

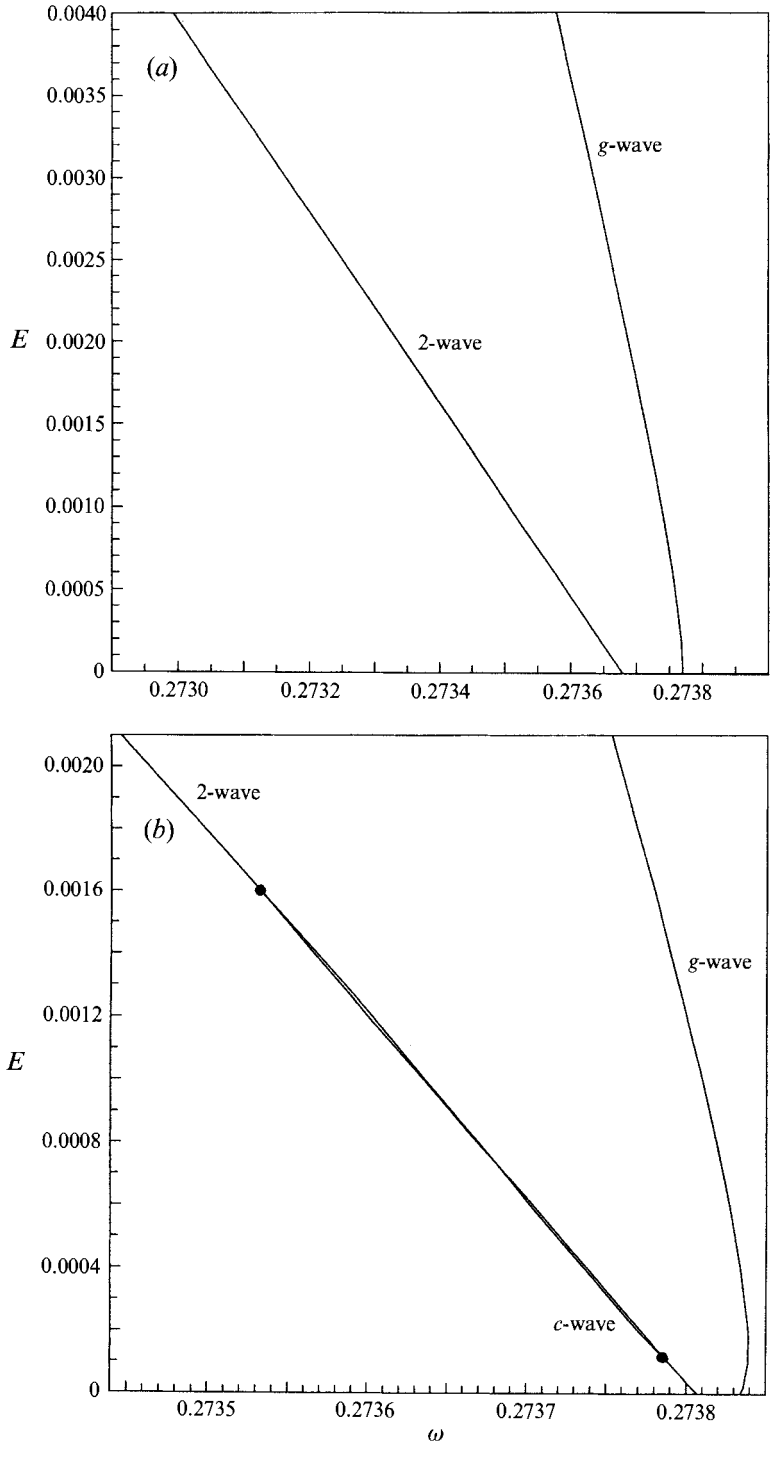

FIGURE 18 (a, b). For caption see facing page.

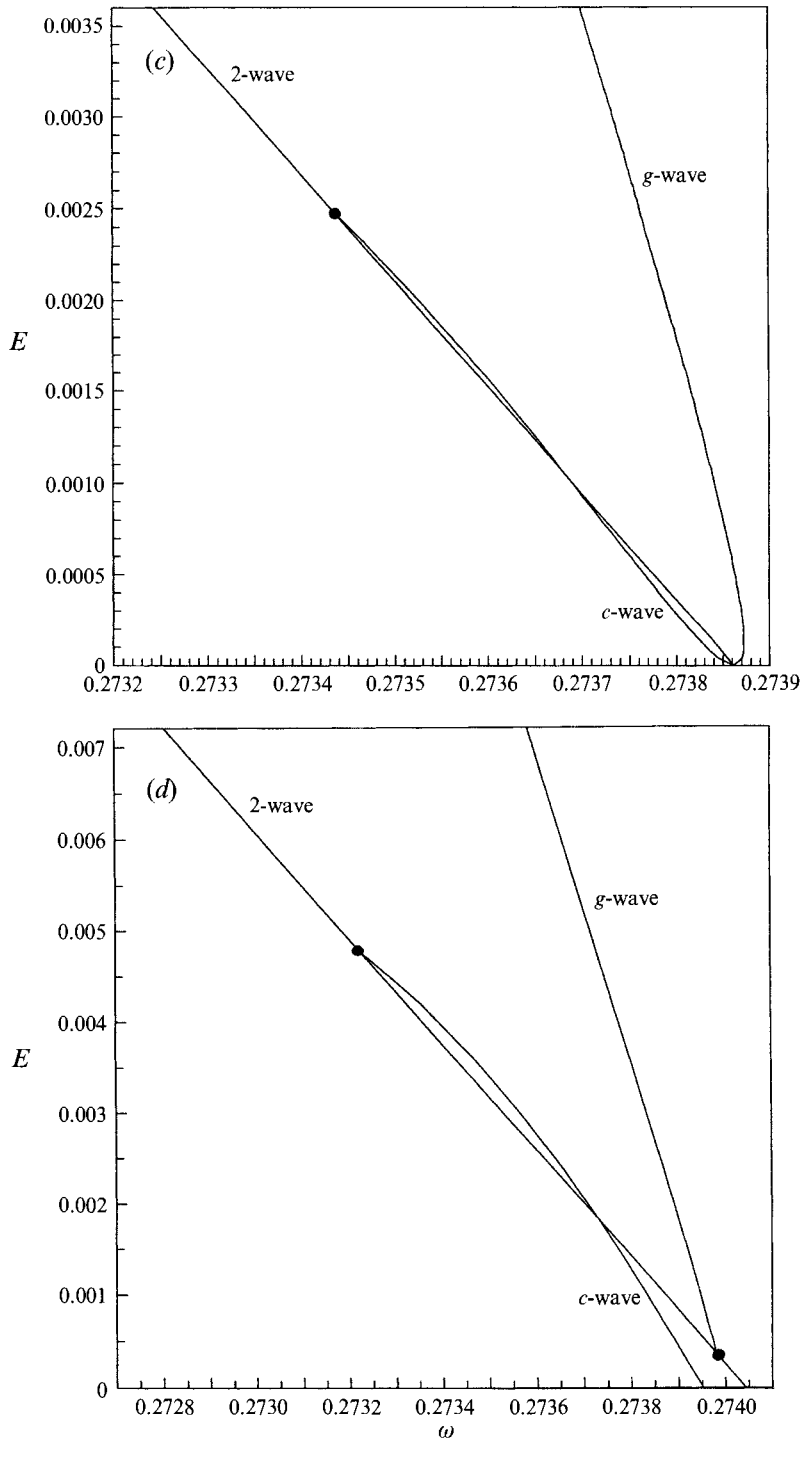

FIGURE 18. *SW* bifurcation diagrams for $\varrho = 0.05$ for (*a*) $b = 0.499$, (*b*) $b = 0.4997$, (*c*) $b = 0.5$ (exact resonance), (*d*) $b = 0.501$. The filled circles indicate bifurcation from a non-trivial solution.

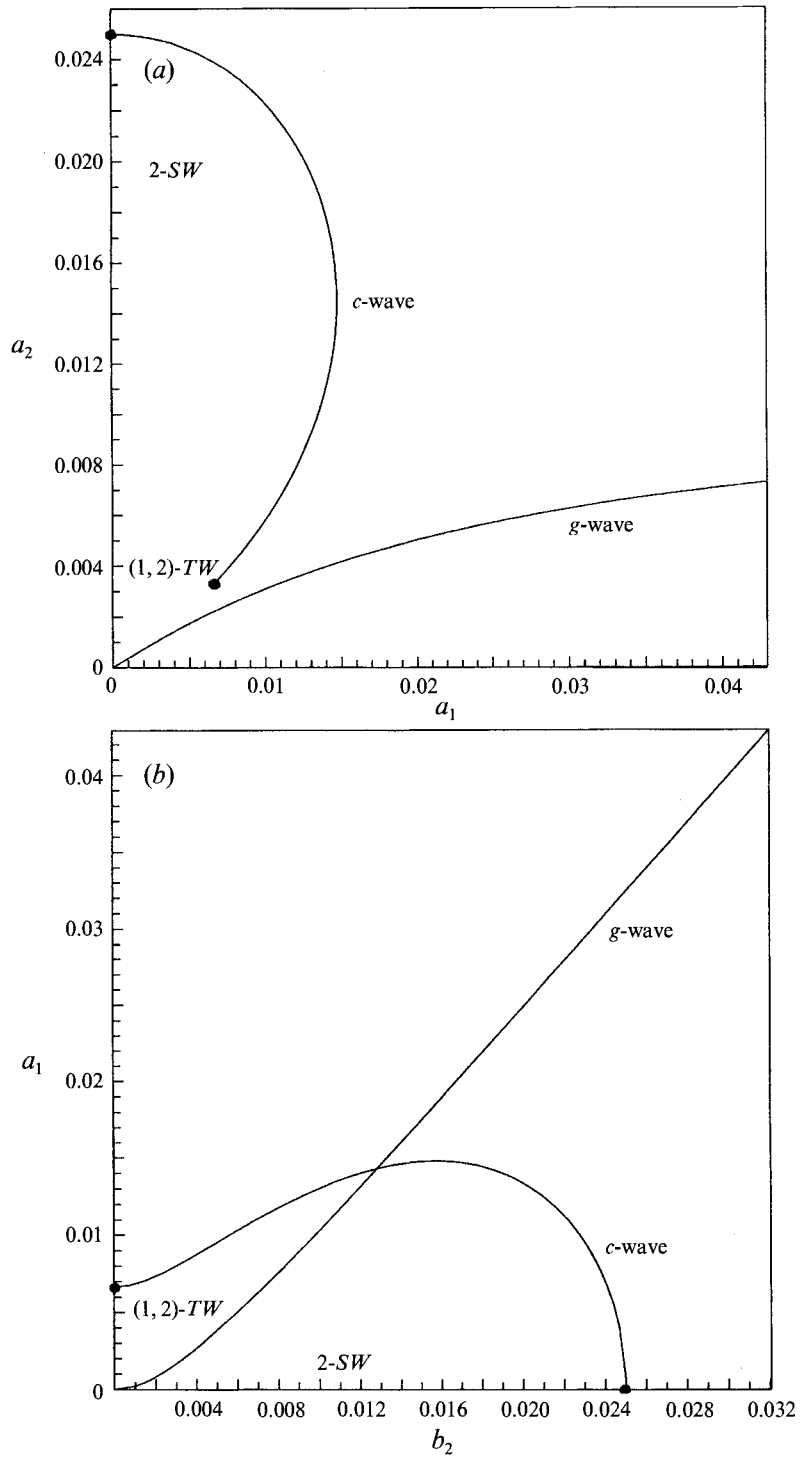

FIGURE 19. Branches of mixed waves (*MW*s) at exact resonance for $\varrho = 0.05$: (*a*) amplitude a_2 versus amplitude a_1 for the two branches of *MW*s, (*b*) amplitude a_1 versus amplitude b_2 for the same branches. The branch of *c-like MW*s bifurcates at one end from the branch of (1,2)-*TW*s and at the other end from the branch of 2-*SW*s.

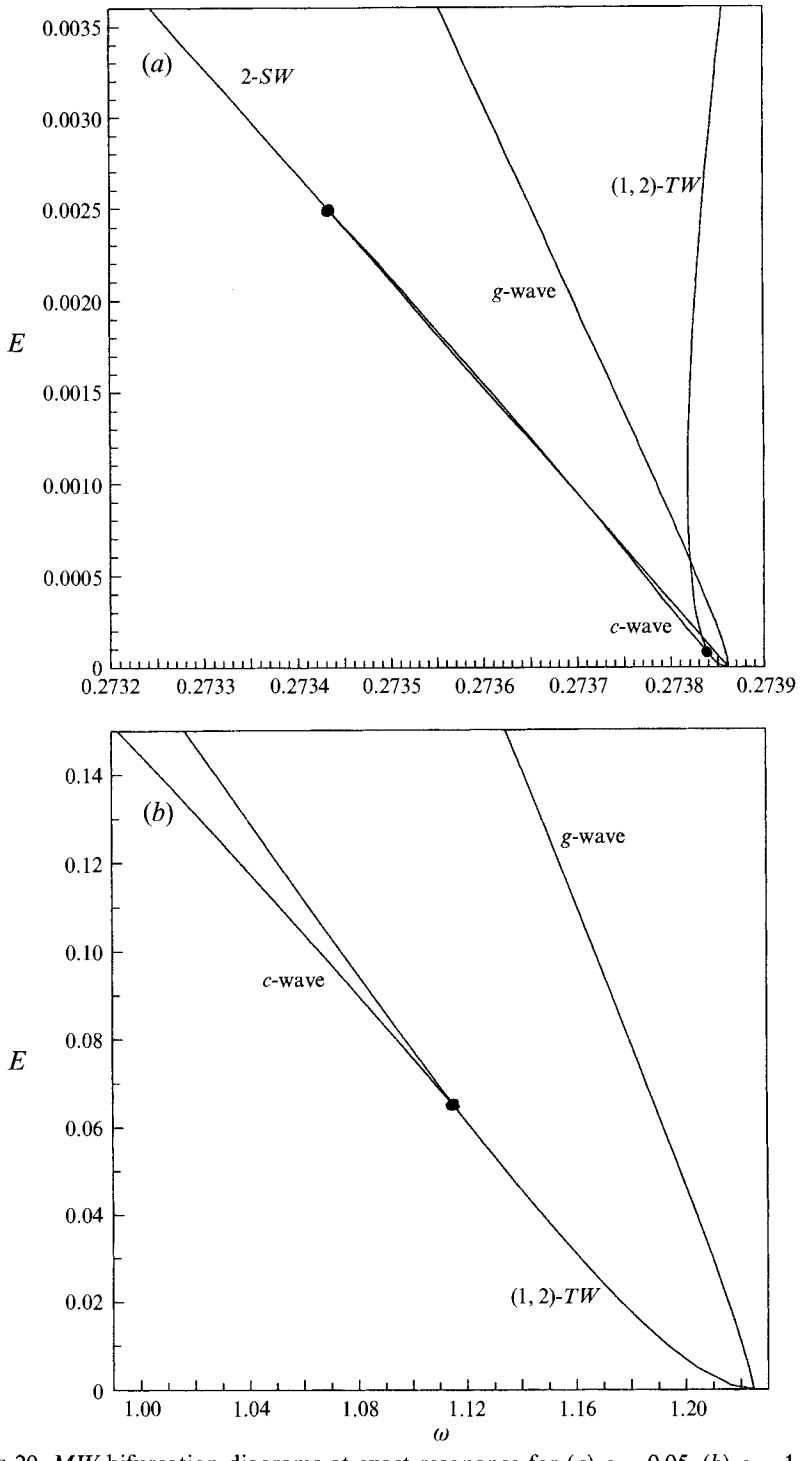

FIGURE 20. *MW* bifurcation diagrams at exact resonance for (*a*) $\varrho = 0.05$, (*b*) $\varrho = 1$ (water waves). The filled circles represent bifurcation points. The branches of waves from which the branch of *c-like MW*s bifurcates are also shown.

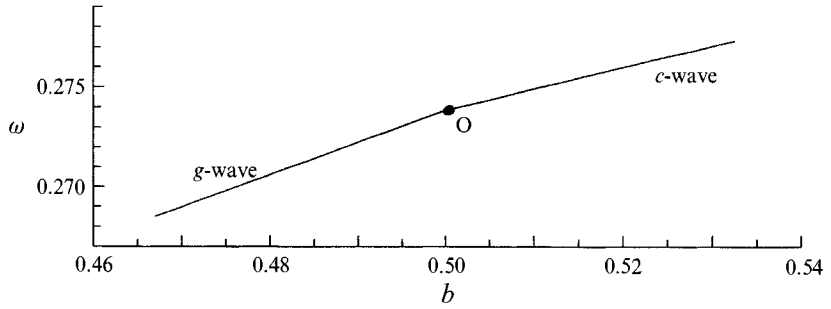

FIGURE 21. Paths of bifurcations points for the *MW*, 2-*TW* and *MW*, (1,2)-*TW* bifurcations for $\varrho = 0.05$. The path on the left of $b = 0.5$ corresponds to the bifurcation from a 2-*TW* to a *MW* of *g-like* type; the path on the right of $b = 0.5$ corresponds to the bifurcation from a (1,2)-*TW* to a *MW* of *c-like* type. The parameter along the path is the energy. The point *O* corresponds to a zero energy.

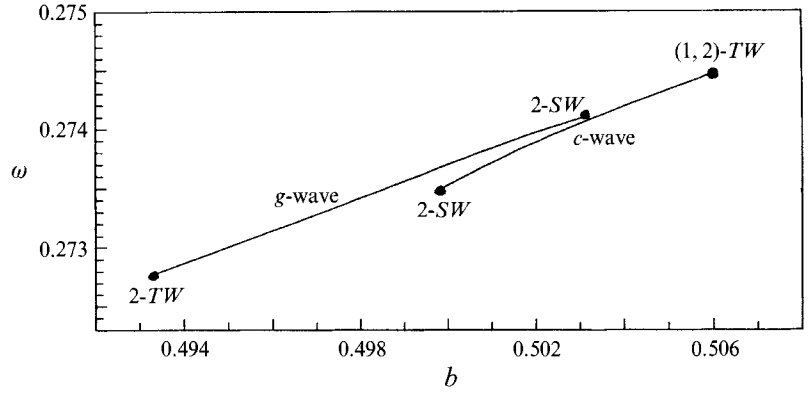

FIGURE 22. Branches of *MW*s for an energy $E = 0.002$ near resonance. The value of ϱ is 0.05. Both branches of *MW*s exist only on a finite interval. From left to right, the coordinates of the bifurcation points (filled circles) are (0.49329,0.27277), (0.49982, 0.27349), (0.50318,0.27410), (0.50609,0.27448).

2-*TW* to a *g-like MW* occurs for values of b smaller than $\frac{1}{2}$ and is shown in figure 21. The bifurcation from a (1,2)-*TW* to a *c-like MW* also occurs. The corresponding path of bifurcation points, which is shown in figure 21, has a turning point at $b = 0.49991$ (which is of course not visible on the plot but explains the bifurcation point at $E = 0.00007$ in figure 20*a*). Next, the value of the energy is fixed and the branches of *MW* are studied as b varies in a neighbourhood of $\frac{1}{2}$. The results are shown in figure 22. The branch of *g-like MW*s bifurcates at one end from the branch of 2-*TW*s and at the other end from the branch of 2-*SW*s. The branch of *c-like MW*s bifurcates at one end from the branch of 2-*SW*s and at the other end from the branch of (1,2)-*TW*s.

6.3. *Discussion on mixed waves*

So far, three-mode mixed waves have been studied only theoretically. Bridges (1990) showed that such waves are generic in the presence of a two-mode interaction and that they persist at any order of the normal-form truncation. A proof of existence of such waves for the full problem remains an open problem (like the proof of existence of standing waves for that matter!). Numerical solutions for such waves would be a first step towards a better description of their nature. What the weakly nonlinear analysis

suggests is that three-mode mixed waves arise from the superposition of a (1,2)-TW^+ and of a 2-TW^- (or vice versa). One may alternatively view such waves as travelling waves in which the fundamental excites not only the second harmonic in the same direction (as in the classical 1:2 resonance for TWs) but also the second harmonic in the opposite direction. Mixed waves can also be found in the no-resonance case but they are degenerate. It should be pointed out that Rayleigh (1915), by investigating whether periodic motions in the form of 'approximate' TWs or SWs at leading order,

$$\eta(x,t) = A(t)\cos x + B(t)\sin x, \qquad \text{with } A \neq B,\ AB \neq 0, \tag{6.11}$$

could be solutions to the water-wave problem was in fact looking for two-mode mixed waves. For gravity waves, Rayleigh concluded negatively. For capillary–gravity waves however, Dias & Bridges (1994) show that, when a certain degeneracy condition is satisfied (see 2.19), waves of the form (6.11) are possible. These waves can be viewed as partially reflected waves and should not be confused with three-mode mixed waves.

7. Time-modulated waves

In the previous sections, only space- and time-periodic motions have been considered. The natural question to ask is whether these waves are stable. A well-known method to study stability is the method of multiple scales. Modulational stability will be discussed in the next section. Here, we only consider the slow time-modulation of the waves. Therefore, the motions are still periodic in space but the amplitudes of the fundamental mode and of the second harmonic are allowed to vary slowly in time. From (A7), one can see how time periodicity has been built into the coefficients. We now assume that the coefficients p_i, q_i, r_i, s_i also depend on time but that this time dependence is slow so that it does not affect the averaging process. As a result (see Dias & Bridges 1994 for a justification), the normal form becomes

$$\left.\begin{aligned}
&\big(\omega^2 - \varrho(1+b)\big)A_1 - \varrho\omega^2\overline{A_1}A_2 - 2\varrho A_1(\alpha_{11}E_1 - \beta_{11}M_1 + \alpha_{12}E_2 - \beta_{12}M_2) = -\mathrm{i}\dot{A}_1,\\
&\big(\omega^2 - \varrho(1+b)\big)B_1 - \varrho\omega^2\overline{B_1}B_2 - 2\varrho B_1(\alpha_{11}E_1 + \beta_{11}M_1 + \alpha_{12}E_2 + \beta_{12}M_2) = -\mathrm{i}\dot{B}_1,\\
&\big(2\omega^2 - \varrho(1+4b)\big)A_2 - \tfrac{1}{2}\varrho\omega^2A_1^2 - 2\varrho A_2(\alpha_{12}E_1 - \beta_{12}M_1 + \alpha_{22}E_2 - \beta_{22}M_2) = -\mathrm{i}\dot{A}_2,\\
&\big(2\omega^2 - \varrho(1+4b)\big)B_2 - \tfrac{1}{2}\varrho\omega^2B_1^2 - 2\varrho B_2(\alpha_{12}E_1 + \beta_{12}M_1 + \alpha_{22}E_2 + \beta_{22}M_2) = -\mathrm{i}\dot{B}_2,
\end{aligned}\right\} \tag{7.1}$$

where the dots mean derivative with respect to t.

The geometrical method used below to study solutions to (7.1) has been applied only recently to dynamical systems. One of the key properties of the system (7.1) is that it has two invariants: $|A_1|^2 + 2|A_2|^2$ and $|B_1|^2 + 2|B_2|^2$, or equivalently $E_1 + 2E_2$ and $M_1 + 2M_2$. Since the method works similarly for TWs and SWs, we describe it for TWs with $B_1 = B_2 = 0$. First (7.1) is rewritten in terms of the real variables E_1, E_2, S, which were already used in the study of periodic solutions in § 2, and of an additional variable $\hat{S} = \mathrm{i}\left(A_1^2\overline{A_2} - \overline{A_1}^2A_2\right)$:

$$\left.\begin{aligned}
\dot{E}_1 &= \varrho\omega^2\hat{S}\\
\dot{E}_2 &= -\tfrac{1}{2}\varrho\omega^2\hat{S}\\
\dot{S} &= \varrho\hat{S}\left[(2b-1) + 2(\alpha_{12} + \beta_{12} - 2\alpha_{11} - 2\beta_{11})E_1 + 2(\alpha_{22} + \beta_{22} - 2\alpha_{12} - 2\beta_{12})E_2\right]\\
\dot{\hat{S}} &= -\varrho S\left[(2b-1) + 2(\alpha_{12} + \beta_{12} - 2\alpha_{11} - 2\beta_{11})E_1 + 2(\alpha_{22} + \beta_{22} - 2\alpha_{12} - 2\beta_{12})E_2\right]\\
&\quad + \varrho\omega^2E_1(4E_2 - E_1).
\end{aligned}\right\} \tag{7.2}$$

In addition to the relation $E_1 + 2E_2 = E$ (constant), there is another obvious relation between the four variables:

$$S^2 + \hat{S}^2 = 4E_1^2 E_2 \quad \text{or} \quad S^2 + \hat{S}^2 = 2E_1^2(E - E_1). \tag{7.3}$$

In the $(S, E_1, \hat{S})$-plane, (7.3) represents a surface of revolution around the E_1-axis, which looks like the surface of a pear. The equation for $\dot{S}$ in (7.2) can be integrated to give

$$\omega^2 S = (2b-1)E_1 + \left[(\alpha_{12} + \beta_{12} - 2\alpha_{11} - 2\beta_{11})E_1^2 - 2(\alpha_{22} + \beta_{22} - 2\alpha_{12} - 2\beta_{12})E_2^2\right] + \mathscr{C}, \tag{7.4}$$

where $\mathscr{C}$ is a constant. In the $(S, E_1, \hat{S})$-plane, (7.4) represents a surface parallel to the $\hat{S}$-axis. The motions lie on the intersection between the surface of revolution (7.3) and the surface (7.4). A description of all possible motions is beyond the scope of this paper and will appear elsewhere (Chossat & Dias 1993).

In this section, we consider what happens when the system is truncated at order two. The surface (7.4) then takes the simple form

$$\omega^2 S = (2b-1)E_1 + \mathscr{C}. \tag{7.5}$$

In the $(S, E_1, \hat{S})$-plane, the motions are given by the intersection of planes parallel to the $\hat{S}$-axis with the surface of the pear. The initial conditions determine the constants E and $\mathscr{C}$. When $|b - \frac{1}{2}|$ is sufficiently small, there are three possible types of motion, which correspond to motions studied by McGoldrick (1970*b*) at exact resonance and by Miles (1976) in a different context: (*a*) the plane is tangent to the pear and consequently the intersection reduces to a point, (*b*) the plane cuts the pear without going through the origin and the resulting intersection is a periodic orbit, (*c*) the plane cuts the pear by going through the origin ($\mathscr{C} = 0$) and the resulting intersection is a homoclinic orbit. Case (*a*) corresponds to the time-periodic motions studied in § 3. There are two planes tangent to the pear, leading to *g-like* ($S > 0$) and *c-like* ($S < 0$) Wilton's ripples. Case (*b*) corresponds to motions with a slow periodic exchange of energy between the fundamental mode and the second harmonic. Case (*c*) is the limit of case (*b*) as the period of exchange of energy becomes infinite. Initially the total energy appears in the fundamental and is ultimately transferred entirely to the second mode. Miles (1976) showed that the equations can be integrated exactly in terms of elliptic functions. If $|b - \frac{1}{2}|$ becomes larger, one of the two periodic motions corresponding to case (*a*) can no longer exist because one of the tangency conditions is no longer satisfied. What happens has been described earlier at the end of § 2: one of the (1,2)-waves becomes a 2-wave. In the $(S, E_1, \hat{S})$-plane, 2-waves all lie at the origin. The other consequence is that the homoclinic orbit can no longer exist. This phenomenon (in a different context) is well illustrated in figure 3 in Miles (1976).

The results for *SW*s are similar to those for *TW*s at second order. A rigorous mathematical analysis of the system (7.1), which includes the effects of higher-order terms, can be found in Chossat & Dias (1993).

8. Discussion

This section provides a discussion on the stability of the travelling waves studied in § 3. In addition, comments are made on the feasibility of experiments to observe such waves. In particular, the effects of viscosity will be briefly discussed.

The modulational stability of a train of weakly nonlinear capillary–gravity water waves has been studied extensively (see for example Hammack & Henderson 1993

for a review of contributions to this field). In infinite depth, the main result at third order is that there is a region of stability for values of b between $(2/\sqrt{3}-1)$ and $\frac{1}{2}$, or for frequencies between 6.4 and 9.8 Hz. When $b = (2/\sqrt{3}-1)$, the second derivative of the frequency ω_0 with respect to k is zero. An internal resonance between the fundamental mode and the Nth harmonic occurs when $b = 1/N$. Therefore, the region of stability includes values of b corresponding to the family of Wilton's ripples down to the 1:6 resonance. The stability results can be obtained by using the method of multiple scales in space and time or the Zakharov equation. Let the free-surface elevation at time $t = 0$ be represented by $\eta(x, t = 0) = \varepsilon A(\varepsilon x)\mathrm{e}^{\mathrm{i}kx}$. At third order, the equation governing the modulations of A is a nonlinear Schrödinger equation of the form

$$2\mathrm{i}\omega_0 A_\tau + \omega_0\omega_0'' A_{\xi\xi} = \frac{gk^3(8+b+2b^2)}{2(1-2b)}A|A|^2, \tag{8.1}$$

where $\tau = \varepsilon^2 t$, $\xi = \varepsilon(x - \omega_0' t)$ (see for example Kawahara 1975 or Djordjevic & Redekopp 1977 for details). A similar equation was also derived by Nayfeh & Saric (1972) for a more general problem (in infinite depth): the space and time modulations of capillary–gravity waves travelling at the interface between two fluids with different densities and in relative motion. Computing the coefficients in their equation (3.39) when there is no relative motion yields

$$2\mathrm{i}\omega_0 A_\tau + \omega_0\omega_0'' A_{\xi\xi} = \frac{\varrho gk^3[4\varrho^2(1+b)^2 + (1-2b)(4+b)]}{2(1-2b)}A|A|^2. \tag{8.2}$$

The previous equation can be referred to as the nonlinear Schrödinger equation governing the modulations of capillary–gravity waves at the interface between two fluids of infinite extent. As far as we know, the results on stability that can be obtained from (8.2) have not appeared elsewhere. The criterion for instability is that the product of the coefficient of the cubic term times the coefficient of $A_{\xi\xi}$ is negative. Figure 23 shows the stability diagram for capillary–gravity interfacial waves. The interesting feature is the curve on the right-hand side, which was first obtained by Dias & Bridges (1994). Along that curve, the coefficient of the cubic term changes sign, and for values of ϱ less than $\frac{3}{4}$, one sees that there is a second region of stability in addition to the unique region of stability for water waves. The derivation of (8.2) as well as (8.1) breaks down near the 1:2 resonance. However, one sees that for small values of ϱ, the region of instability is very small in a neighbourhood of $b = \frac{1}{2}$. In order to study the stability in that neighbourhood one needs a different scaling of the amplitudes. Jones (1992) studied the stability of Wilton's ripples in the case of water waves and obtained a system of two coupled nonlinear partial differential equations governing the modulations of the amplitudes of the fundamental and of its second harmonic. Jones found that Wilton's ripples are always unstable to perturbations in the same direction as the ripple. Note however that his analysis is restricted to exact resonance and does not allow for a detuning. Nayfeh & Saric (1972) also considered the second-harmonic resonance for Kelvin–Helmholtz waves. But their equations, which are first order in time and in space, are essentially the same as McGoldrick's (1970*b*). A stability analysis in the spirit of Jones' analysis can certainly be extended to interfacial waves and be modified to include near-resonant waves, but it is beyond the scope of our paper. However, in view of the stabilizing role played by the density ratio as it approaches unity for capillary–gravity waves away from resonance, one might anticipate a stabilizing role for Wilton's ripples too.

Wilton's ripples have also been studied experimentally in the case of water waves.

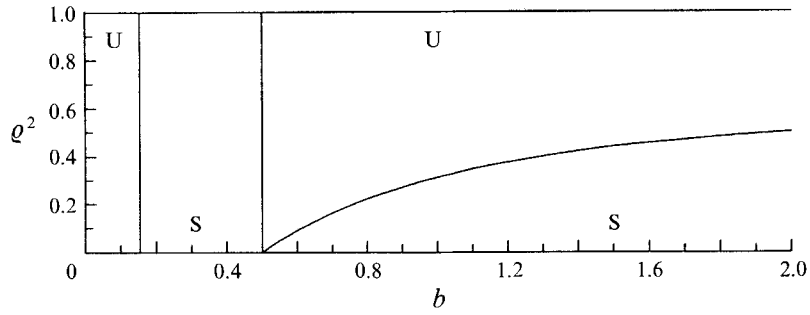

FIGURE 23. Stability diagram for interfacial capillary–gravity waves (S: stable, U: unstable).

McGoldrick (1970*a*) generated Wilton's ripples but used tap water and discovered that a surface film was present (see the discussion below on the effects of viscosity and surfactants). His waves were rapidly attenuated and did not even reach the end of the basin. Researchers who have performed experiments on Wilton's ripples have noticed that they can be excited even if the wave steepness is quite small and if there is important detuning. Hammack & Henderson (1993) report that internal resonances occur in the whole region of modulational stability, which was described above and corresponds to frequencies in the range [6.4, 9.8] Hz. Moreover, the timescales on which they evolve are different from the predictions of resonant interaction theory. Therefore, one must be cautious when using analytical results on stability in the internal resonance region. Perlin & Ting (1992) also performed experiments in the same frequency range, with an emphasis on steep waves. It is interesting to note that only *g-like* waves seem to be observed in experiments, perhaps because of the modulational instability present in the region $b > \frac{1}{2}$ (*c-like* waves).

As far as we are aware, no stability analysis for capillary–gravity standing waves and no experiments on standing Wilton's ripples have been performed.

Experiments on capillary–gravity interfacial waves have been done, in particular when there is a relative motion between the two fluids. Thorpe (1969) and Pouliquen *et al.* (1992) have performed the Reynolds experiment which consists of tilting a tube filled with two immiscible fluids, thus creating a shear flow. Of course the purpose of the experiment is not directly related to the present study, but an inviscid theory seems to be appropriate to describe the waves they observe. Moreover, for the fluids used in their experiments, the wavelength corresponding to the 1:2 resonance is between 2.6 and 9 cm, with corresponding frequency between 1 and 2.8 Hz. These are 'realistic' wavelengths and frequencies. Again in the context of Kelvin–Helmholtz waves, Bontozoglou & Hanratty (1990) have shown that the 1:2 resonance can explain some of the observed phenomena in gas–liquid flows.

In experiments, viscosity and surfactants can play an important role. Viscous dissipation can be incorporated in the equations for the wave propagation. Miles (1988) and Joo, Messiter & Schultz (1991), following Lamb's analysis (see Lamb 1932, Art. 348), show that viscous dissipation appears at third order and leads to a modified version of (8.1):

$$2\mathrm{i}\omega_0 A_\tau + 2\mathrm{i}\omega_0^2 \alpha A + \omega_0 \omega_0'' A_{\xi\xi} = \frac{gk^3(8+b+2b^2)}{2(1-2b)} A|A|^2, \tag{8.3}$$

where

$$\alpha = \frac{2\nu k^2}{\varepsilon^2 \omega_0}, \tag{8.4}$$

and ν denotes the kinematic viscosity. McGoldrick (1970*a*) also includes viscous damping in his second-order equations. But the damping coefficient $D = \alpha\varepsilon^2$ is of order ε^2 and therefore is consistent with (8.3). Joo *et al.* treat the effect of surfactants but use a different scaling between the wave amplitude and the boundary-layer thickness so that the dissipation due to surfactants also appears at third order and they conclude that surfactants have no effects on Wilton's ripples. But in fact the damping coefficient is much stronger for surfactants (for water, the damping factor due to viscosity is equal to 0.0021 while the damping factor due to surfactants is 0.011) and that explains why McGoldrick observed such a rapid attenuation of his waves. Extending Lamb's analysis to interfacial waves, one can expect a similar behaviour with ν in (8.4) replaced by $(\mu + \mu')/(\rho + \rho')$, where μ and μ' are the viscosities of the fluids.

The discussion above indicates that experiments may be performed successfully to study resonant interfacial capillary–gravity waves. In addition to the difficulties associated with experimental capillary–gravity water waves (accurate measure of the surface tension coefficient, dissipation due to viscosity and contamination of the free surface), there is, for interfacial waves, the difficulty of finding immiscible fluids. However, preliminary results on stability indicate a stabilizing effect of the density ratio as it approaches unity.

Appendix A. Derivation of the functional $\mathscr{L}$

With the restriction to space-periodic functions, the canonical variables $\eta(x,t)$ and $\zeta(x,t)$ can be formally identified with Fourier series expansions in space. Taking zero as average wave elevation, $1/k$ as unit length and $(gk)^{\frac{1}{2}}$ as unit frequency, a wave with wavenumber k is represented by the Fourier series expansions

$$\eta(x,t) = \sum_{n=1}^{\infty} (A_n(t)\cos nx + B_n(t)\sin nx)\,, \tag{A 1}$$

$$\zeta(x,t) = \zeta_0(t) + \sum_{n=1}^{\infty} (C_n(t)\cos nx + D_n(t)\sin nx)\,, \tag{A 2}$$

where ζ has been non-dimensionalized by being divided by $(\rho + \rho')(gk)^{\frac{1}{2}}/k^2$.

Restricting the Fourier series to a finite number of terms N, Dias & Bridges (1994) have shown that the kinetic energy defined in (2.6) can be represented in a convenient matrix form

$$K(\zeta,\eta) = K(\{\zeta\},\{\eta\}) = \frac{(\rho+\rho')^2 g}{2\pi k^3}\{\zeta\}^T[P]^{-1}\{\zeta\}, \tag{A 3}$$

where $\{\eta\}$ and $\{\zeta\}$ are $2N$-dimensional, time-dependent vectors of Fourier coefficients and the $2N \times 2N$ matrix $[P]$ depends only on ρ, ρ' and the Fourier coefficients of $\eta(x,t)$. Eliminating the vector $\{\zeta\}$ by using (2.9) yields

$$\{\eta_t\} = \frac{\rho+\rho'}{\pi}[P]^{-1}\{\zeta\} \quad \text{or} \quad \{\zeta\} = \frac{\pi}{\rho+\rho'}[P]\{\eta_t\}. \tag{A 4}$$

Therefore the Lagrangian $K - V$ can be expressed purely in terms of the Fourier

coefficients of $\eta(x,t)$:

$$K - V = \frac{\pi g}{2k^3}\{\eta_t\}^T[P]\{\eta_t\} - V\,. \tag{A 5}$$

Away from resonance, it is sufficient to take $N = 2$ in order to study space- and time-periodic waves with small energy (Dias & Bridges 1994). However, in the presence of resonance, at least $N = 4$ terms need to be retained. Using the Fourier series expansions for η given in (A1) with $N = 4$, one finds that the matrix $[P]$ is equal to

$$[P] = \rho[P^+] + \rho'[P^-] \quad \text{with} \quad [P^\pm] = \begin{bmatrix} [P_1^\pm] & [P_2^\pm] \\ [P_2^\pm]^T & [P_3^\pm] \end{bmatrix},$$

where

$$[\mathrm{P}_1^\pm] = \begin{bmatrix} 1 \pm A_2 + \frac{1}{4}(A_1^2 - B_1^2) + \frac{1}{2}(A_2^2 + B_2^2) & \pm A_3 + \frac{1}{2}(A_1A_2 - B_1B_2) & \pm A_4 + \frac{1}{4}(A_2^2 - B_2^2) & 0 \\ \pm A_3 + \frac{1}{2}(A_1A_2 - B_1B_2) & \frac{1}{2} \pm A_4 + \frac{1}{2}(A_2^2 - B_2^2) & 0 & 0 \\ \pm A_4 + \frac{1}{4}(A_2^2 - B_2^2) & 0 & \frac{1}{3} & 0 \\ 0 & 0 & 0 & \frac{1}{4} \end{bmatrix},$$

$$[\mathrm{P}_2^\pm] = \begin{bmatrix} \pm B_2 + \frac{1}{2}A_1B_1 & \pm B_3 + \frac{1}{2}(A_1B_2 + B_1A_2) & \pm B_4 + \frac{1}{2}A_2B_2 & 0 \\ \pm B_3 + \frac{1}{2}(A_1B_2 + B_1A_2) & \pm B_4 + A_2B_2 & 0 & 0 \\ \pm B_4 + \frac{1}{2}A_2B_2 & 0 & 0 & 0 \\ 0 & 0 & 0 & 0 \end{bmatrix},$$

$$[\mathrm{P}_3^\pm] = \begin{bmatrix} 1 \mp A_2 - \frac{1}{4}(A_1^2 - B_1^2) + \frac{1}{2}(A_2^2 + B_2^2) & \mp A_3 - \frac{1}{2}(A_1A_2 - B_1B_2) & \mp A_4 - \frac{1}{4}(A_2^2 - B_2^2) & 0 \\ \mp A_3 - \frac{1}{2}(A_1A_2 - B_1B_2) & \frac{1}{2} \mp A_4 - \frac{1}{2}(A_2^2 - B_2^2) & 0 & 0 \\ \mp A_4 - \frac{1}{4}(A_2^2 - B_2^2) & 0 & \frac{1}{3} & 0 \\ 0 & 0 & 0 & \frac{1}{4} \end{bmatrix}.$$

Once $[P]$ has been obtained, (A5) yields the Lagrangian, correct up to fourth order:

$$\begin{aligned} K - V = {} & \tfrac{1}{2}\pi(\rho + \rho')gk^{-3}\left[\dot{A}_1^2 + \dot{B}_1^2 + \tfrac{1}{2}\dot{A}_2^2 + \tfrac{1}{2}\dot{B}_2^2 + \dot{A}_1\dot{B}_1A_1B_1 + \tfrac{1}{4}(\dot{A}_1^2 - \dot{B}_1^2)(A_1^2 - B_1^2)\right. \\ & + \varrho(A_2\dot{A}_1^2 - A_2\dot{B}_1^2 + 2B_2\dot{A}_1\dot{B}_1) + \tfrac{1}{2}(\dot{A}_1^2 + \dot{B}_1^2)(A_2^2 + B_2^2) \\ & + (\dot{A}_1\dot{A}_2 - \dot{B}_1\dot{B}_2)(A_1A_2 - B_1B_2) + (\dot{A}_1\dot{B}_2 + \dot{A}_2\dot{B}_1)(A_1B_2 + A_2B_1) \\ & + 2\dot{A}_2\dot{B}_2A_2B_2 + \tfrac{1}{2}(\dot{A}_2^2 - \dot{B}_2^2)(A_2^2 - B_2^2) + \tfrac{1}{3}(\dot{A}_3^2 + \dot{B}_3^2) + \tfrac{1}{4}(\dot{A}_4^2 + \dot{B}_4^2) \\ & \left. + 2\varrho(\dot{A}_1\dot{A}_2A_3 - \dot{B}_1\dot{B}_2A_3 + \dot{A}_1\dot{B}_2B_3 + \dot{A}_2\dot{B}_1B_3 + \tfrac{1}{2}\dot{A}_2^2A_4 - \tfrac{1}{2}\dot{B}_2^2A_4 + \dot{A}_2\dot{B}_2B_4)\right] \\ & - \tfrac{1}{2}\pi(\rho - \rho')gk^{-3}\left[(1 + b)(A_1^2 + B_1^2) + (1 + 4b)(A_2^2 + B_2^2)\right. \\ & \qquad \left. + (1 + 9b)(A_3^2 + B_3^2) + (1 + 16b)(A_4^2 + B_4^2)\right. \\ & \left. - \tfrac{3}{16}b(A_1^2 + B_1^2)^2 - 3b(A_2^2 + B_2^2)^2 - 3b(A_1^2 + B_1^2)(A_2^2 + B_2^2)\right]. \end{aligned} \tag{A 6}$$

The problem has been reduced to a finite-dimensional Hamiltonian system with eight degrees of freedom. Next, we expand the eight Fourier coefficients A_n, B_n $(n = 1, 2, 3, 4)$ in Fourier series in time. The simplest Fourier expansions that result in a complete local theory are

$$\left.\begin{aligned} A_1 &= p_1\cos\omega t + q_1\sin\omega t + t_1^3\cos 3\omega t + u_1^3\sin 3\omega t, \\ B_1 &= r_1\cos\omega t + s_1\sin\omega t + v_1^3\cos 3\omega t + w_1^3\sin 3\omega t, \\ A_2 &= p_2\cos 2\omega t + q_2\sin 2\omega t + x_2, \\ B_2 &= r_2\cos 2\omega t + s_2\sin 2\omega t + y_2, \\ A_3 &= t_3\cos 3\omega t + u_3\sin 3\omega t + t_3^1\cos\omega t + u_3^1\sin\omega t, \\ B_3 &= v_3\cos 3\omega t + w_3\sin 3\omega t + v_3^1\cos\omega t + w_3^1\sin\omega t, \\ A_4 &= t_4\cos 4\omega t + u_4\sin 4\omega t + x_4, \\ B_4 &= v_4\cos 4\omega t + w_4\sin 4\omega t + y_4, \end{aligned}\right\} \tag{A 7}$$

where ω is the dimensionless frequency of the wave. Substituting (A7) into (A6), integrating over time and dividing by (2.10) results in the functional

$$\mathscr{L} = \left(\omega^2 - \varrho(1+b)\right) E_1 + \left(2\omega^2 - \varrho(1+4b)\right) E_2 + \tfrac{1}{8}\omega^2 \left(E_1^2 - 3M_1^2\right) + \omega^2 \left(E_2^2 - 3M_2^2\right) + \tfrac{3}{2}\varrho b \left(\tfrac{3}{16}E_1^2 - \tfrac{1}{16}M_1^2 + 3E_2^2 - M_2^2 + 2E_1E_2\right) - \tfrac{1}{2}\varrho\omega^2 S + f(t,u,v,w,x,y), \qquad (A\,8)$$

where f is a lengthy function of the coefficients t, u, v, w, x, y and

$$E_i = \tfrac{1}{2}(p_i^2 + q_i^2 + r_i^2 + s_i^2) \qquad (i = 1,2),$$
$$M_i = q_i r_i - p_i s_i \qquad (i = 1,2),$$
$$S = \tfrac{1}{2}p_2(p_1^2 - q_1^2 - r_1^2 + s_1^2) + q_2(p_1q_1 - r_1s_1) + r_2(p_1r_1 - q_1s_1) + s_2(p_1s_1 + q_1r_1).$$

The above expression for the reduced functional is a generalization of the expression that Dias & Bridges (1994) obtained for the study of space- and time-periodic interfacial waves without resonance. If one sets all the coefficients t, u, v, w and x_4, y_4 to zero in (A8), $\mathscr{L}$ reduces to the expression in Dias & Bridges. In the no-resonance case, the coefficients of A_2 and B_2 are then eliminated in terms of the coefficients of A_1 and B_1. In the case of the 1:2 resonance, however, the coefficients to be eliminated are the coefficients of A_3, B_3, A_4 and B_4 (and also the 'constant' coefficients in A_2 and B_2). Therefore, the next step is to eliminate the coefficients t, u, v, w, x, y in terms of the coefficients p, q, r, s. Because of the symmetries of the problem, the coefficients p, q, r, s appear only in the combinations E_1, E_2, M_1, M_2, S (see Bridges 1990 for a proof). We find that the reduced functional $\mathscr{L}(E_1, M_1, E_2, M_2, S, \omega; b, \varrho)$ takes the form

$$\mathscr{L} = \left(\omega^2 - \varrho(1+b)\right) E_1 + \left(2\omega^2 - \varrho(1+4b)\right) E_2 - \tfrac{1}{2}\varrho\omega^2 S - \varrho\left[\alpha_{11}E_1^2 + \beta_{11}M_1^2 + \alpha_{22}E_2^2 + \beta_{22}M_2^2 + 2\alpha_{12}E_1E_2 + 2\beta_{12}M_1M_2\right], \qquad (A\,9)$$

where the full expressions for the coefficients α_{ij} and β_{ij}, which depend only on b, ϱ and ω^2, can be found in appendix B.

In order to see the connection with travelling and standing waves, we consider the order-one expansion of η (see (A1) with $N = 2$):

$$\eta = A_1(t)\cos x + B_1(t)\sin x + A_2(t)\cos 2x + B_2(t)\sin 2x.$$

If we expand the coefficients A_1, B_1, A_2, B_2 in time t (see (A7)) and retain only the first-order terms, we obtain

$$\eta = (p_1\cos\omega t + q_1\sin\omega t)\cos x + (r_1\cos\omega t + s_1\sin\omega t)\sin x + (p_2\cos 2\omega t + q_2\sin 2\omega t)\cos 2x + (r_2\cos 2\omega t + s_2\sin 2\omega t)\sin 2x,$$

or

$$\eta = \mathrm{Re}\left[\tilde{A}_1 e^{-i(\omega t - x)} + \tilde{B}_1 e^{-i(\omega t + x)} + \tilde{A}_2 e^{-i(2\omega t - 2x)} + \tilde{B}_2 e^{-i(2\omega t + 2x)}\right], \qquad (A\,10)$$

where

$$\left.\begin{aligned} \tilde{A}_i &= \tfrac{1}{2}(p_i + s_i) + \tfrac{1}{2}i(q_i - r_i) \\ \tilde{B}_i &= \tfrac{1}{2}(p_i - s_i) + \tfrac{1}{2}i(q_i + r_i) \end{aligned}\right\} \qquad (i = 1,2).$$

It is clear from (A10) that if $\tilde{B}_1 = \tilde{B}_2 = 0$, resp. $\tilde{A}_1 = \tilde{A}_2 = 0$, the solution is an interfacial *TW* travelling to the right, resp. left. If $|\tilde{A}_1| = |\tilde{B}_1|$ and $|\tilde{A}_2| = |\tilde{B}_2|$, the solution is an interfacial *SW*. The corresponding quantities E_1, M_1, E_2, M_2 and S are given in (2.12)–(2.14). Note that in the main text, we have omitted the tilde.

Appendix B. Coefficients in the normal form

The general expressions for the coefficients α_{ij} and β_{ij}, which appear in the expression of the reduced functional $\mathscr{L}$ (2.11), are

$$\alpha_{11} = -\frac{9b}{32} - \frac{\omega^2}{8\varrho} - \frac{\omega^4}{4(1+4b)},$$

$$\beta_{11} = \frac{3b}{32} + \frac{3\omega^2}{8\varrho} + \frac{\omega^4}{4(1+4b)},$$

$$\alpha_{12} = -\frac{3b}{2} - \frac{\omega^2}{4\varrho} + \frac{\varrho\omega^4}{3\omega^2-(1+9b)\varrho} + \frac{3\varrho\omega^4}{\omega^2-3(1+9b)\varrho} + \frac{9\varrho\omega^4}{36\omega^2-4(1+b)\varrho},$$

$$\beta_{12} = \frac{\omega^2}{\varrho} + \frac{\varrho\omega^4}{3\omega^2-(1+9b)\varrho} - \frac{3\varrho\omega^4}{\omega^2-3(1+9b)\varrho} - \frac{9\varrho\omega^4}{36\omega^2-4(1+b)\varrho},$$

$$\alpha_{22} = -\frac{9b}{2} - \frac{\omega^2}{\varrho} - \frac{4\omega^4}{1+16b} + \frac{2\varrho\omega^4}{4\omega^2-(1+16b)\varrho},$$

$$\beta_{22} = \frac{3b}{2} + \frac{3\omega^2}{\varrho} + \frac{4\omega^4}{1+16b} + \frac{2\varrho\omega^4}{4\omega^2-(1+16b)\varrho}.$$

Since the coefficients α_{ij} and β_{ij} only appear in the cubic terms in the normal form, the frequency ω can be replaced by the linear frequency ω_0. For 1-waves or combination waves, the linear frequency is given by $\omega_0^2 = \varrho(1+b)$. For 2-waves, it is given by $\omega_0^2 = \frac{1}{2}\varrho(1+4b)$. The simplified expressions for the coefficients are given below.

B.1. *Simplified expression for* 1*-waves and* (1, 2)*-waves*

$$\alpha_{11} = -\frac{4+13b}{32} - \frac{(1+b)^2}{4(1+4b)}\varrho^2,$$

$$\beta_{11} = \frac{3(4+5b)}{32} + \frac{(1+b)^2}{4(1+4b)}\varrho^2,$$

$$\alpha_{12} = -\frac{1+7b}{4} - \frac{(1+b)(23-410b-b^2)}{32(1-3b)(1+13b)}\varrho^2,$$

$$\beta_{12} = 1+b+\frac{(1+b)(55+38b+415b^2)}{32(1-3b)(1+13b)}\varrho^2,$$

$$\alpha_{22} = -\frac{2+11b}{2} - \frac{10(1+b)^2(1-8b)}{3(1-4b)(1+16b)}\varrho^2,$$

$$\beta_{22} = \frac{3(2+3b)}{2} + \frac{2(1+b)^2(7-8b)}{3(1-4b)(1+16b)}\varrho^2.$$

Note that the denominators of the coefficients α_{12} and β_{12} vanish when $b = \frac{1}{3}$: this phenomenon is associated with the resonance between the fundamental mode and the third harmonic. The ordering of the Fourier coefficients used here is no longer valid. Similarly, the denominators of the coefficients α_{22} and β_{22} vanish when $b = \frac{1}{4}$, i.e. when the fundamental mode and the fourth harmonic resonate.

B.2. *Simplified expression for* 2*-waves*

$$\alpha_{22} = -\frac{1+13b}{2} - \frac{(1-32b)(1+4b)^2}{2(1-8b)(1+16b)}\varrho^2,$$

$$\beta_{22} = \frac{3(1+5b)}{2} + \frac{3(1+4b)^2}{2(1-8b)(1+16b)}\varrho^2 .$$

Note that the other coefficients are not needed.

Appendix C. Coefficients for the total energy

The general expressions for the coefficients α_{ij}^H and β_{ij}^H, which appear in the expression of the total energy $\mathscr{H}$ (2.17), are

$$\alpha_{11}^H = -\frac{27b}{32} - \frac{\omega^2}{8\varrho} + \frac{\omega^4}{4(1+4b)},$$

$$\beta_{11}^H = \frac{9b}{32} + \frac{3\omega^2}{8\varrho} - \frac{\omega^4}{4(1+4b)},$$

$$\alpha_{12}^H = -\frac{9b}{2} - \frac{\omega^2}{4\varrho} + \frac{\varrho\omega^4[3\omega^2+(1+9b)\varrho]}{[3\omega^2-(1+9b)\varrho]^2} + \frac{3\varrho\omega^4[\omega^2+3(1+9b)\varrho]^2}{[\omega^2-3(1+9b)\varrho]^2} + \frac{9\varrho\omega^4[9\omega^2+(1+b)\varrho]}{4[9\omega^2-(1+b)\varrho]^2},$$

$$\beta_{12}^H = \frac{\omega^2}{\varrho} + \frac{\varrho\omega^4[3\omega^2+(1+9b)\varrho]}{[3\omega^2-(1+9b)\varrho]^2} - \frac{3\varrho\omega^4[\omega^2+3(1+9b)\varrho]^2}{[\omega^2-3(1+9b)\varrho]^2} - \frac{9\varrho\omega^4[9\omega^2+(1+b)\varrho]}{4[9\omega^2-(1+b)\varrho]^2},$$

$$\alpha_{22}^H = -\frac{27b}{2} - \frac{\omega^2}{\varrho} + \frac{4\omega^4}{1+16b} + \frac{2\varrho\omega^4[4\omega^2+(1+16b)\varrho]}{[4\omega^2-(1+16b)\varrho]^2},$$

$$\beta_{22}^H = \frac{9b}{2} + \frac{3\omega^2}{\varrho} - \frac{4\omega^4}{1+16b} + \frac{2\varrho\omega^4[4\omega^2+(1+16b)\varrho]}{[4\omega^2-(1+16b)\varrho]^2}.$$

Since the coefficients α_{ij}^H and β_{ij}^H only appear in the fourth-order terms in $\mathscr{H}$, the frequency ω can be replaced by the linear frequency ω_0. For 1-waves or combination waves, the linear frequency is given by $\omega_0^2 = \varrho(1+b)$. For 2-waves, it is given by $\omega_0^2 = \frac{1}{2}\varrho(1+4b)$.

REFERENCES

ASTON, P. J. 1991 Local and global aspects of the $(1,n)$ mode interaction for capillary–gravity waves. *Physica* D **52**, 415–428.

ASTON, P. J. 1993 Understanding the global solutions of the capillary–gravity wave problem. *Wave Motion* **17**, 113–141.

BARAKAT, R. & HOUSTON, A. 1968 Nonlinear periodic capillary–gravity waves on a fluid of finite depth. *J. Geophys. Res.* **73**, 6545–6555.

BENJAMIN, T. B. & BRIDGES, T. J. 1991 Reappraisal of the Kelvin–Helmholtz problem. Preprint, Oxford University.

BOHR, N. 1906 See *Collected Works*, Vol. 1, pp. 67–78. North-Holland (1972).

BONTOZOGLOU, V. & HANRATTY, T. J. 1990 Capillary–gravity Kelvin–Helmholtz waves close to resonance. *J. Fluid Mech.* **217**, 71–91.

BRIDGES, T. J. 1990 $\mathbf{O}(2)$-invariant Hamiltonians on $\mathbb{C}^4$ and the (m,n) mode-interaction problem for capillary–gravity waves. *Stud. Appl. Maths* **82**, 93–120.

CHEN, B. & SAFFMAN, P. G. 1979 Steady gravity–capillary waves on deep water-I. Weakly nonlinear waves. *Stud. Appl. Maths* **60**, 183–210.

CHEN, B. & SAFFMAN, P. G. 1980 Steady gravity–capillary waves on deep water-II. Numerical results for finite amplitude. *Stud. Appl. Maths* **62**, 95–111.

CHOSSAT, P. & DIAS, F. 1993 A geometrical study of 1:2 resonance in Hamiltonian systems with $\mathbf{O}(2)$ symmetry. Preprint, Institut Non-Linéaire de Nice.

CRAIK, A. D. D. 1985 *Wave Interactions and Fluid Flows*. Cambridge University Press.

DIAS, F. & BRIDGES, T. J. 1994 Geometric aspects of spatially periodic interfacial waves. *Stud. Appl. Maths*, to appear.

DIXON, A. 1990 A stability analysis for interfacial waves using a Zakharov equation. *J. Fluid Mech.* **214**, 185–210.

DJORDJEVIC, V. D. & REDEKOPP, L. G. 1977 On two-dimensional packets of capillary–gravity waves. *J. Fluid Mech.* **79**, 703–714.

GRIMSHAW, R. H. J. & PULLIN, D. I. 1985 Stability of finite-amplitude interfacial waves. Part 1. Modulational instability for small-amplitude waves. *J. Fluid Mech.* **160**, 297–315.

HAMMACK, J. L. & HENDERSON, D. M. 1993 Resonant interactions among surface water waves. *Ann. Rev. Fluid Mech.* **25**, 55–97.

HARRISON, W. J. 1909 The influence of viscosity and capillarity on waves of finite amplitude. *Proc. Lond. Math. Soc.* **7**, 107–121.

HENDERSON, D. M. & HAMMACK, J. L. 1987 Experiments on ripple instabilities. Part 1. Resonant triads. *J. Fluid Mech.* **184**, 15–41.

HOGAN, S. J. 1981 Some effects of surface tension on steep water waves. Part 3. *J. Fluid Mech.* **110**, 381–410.

JONES, M. C. W. 1989 Small amplitude capillary–gravity waves in a channel of finite depth. *Glasgow Math. J.* **31**, 141–160.

JONES, M. C. W. 1992 Nonlinear stability of resonant capillary–gravity waves. *Wave Motion* **15**, 267–283.

JONES, M. C. W. & TOLAND, J. F. 1986 Symmetry and the bifurcation of capillary–gravity waves. *Arch. Rat. Mech. Anal.* **96**, 29–53.

JOO, S. W., MESSITER, A. F. & SCHULTZ, W. W. 1991 Evolution of weakly nonlinear water waves in the presence of viscosity and surfactant. *J. Fluid Mech.* **229**, 135–158.

KAWAHARA, T. 1975 Nonlinear self-modulation of capillary–gravity waves on a liquid layer. *J. Phys. Soc. Japan* **38**, 265–270.

LAMB, H. 1932 *Hydrodynamics.* Cambridge University Press.

MCGOLDRICK, L. F. 1970*a* An experiment on second-order capillary gravity resonant wave interactions. *J. Fluid Mech.* **40**, 251–271.

MCGOLDRICK, L. F. 1970*b* On Wilton's ripples: a special case of resonant interactions. *J. Fluid Mech.* **42**, 193–200.

MILES, J. W. 1976 Nonlinear surface waves in closed basins. *J. Fluid Mech.* **75**, 419-448.

MILES, J. W. 1986 Weakly nonlinear Kelvin–Helmholtz waves. *J. Fluid Mech.* **172**, 513–529.

MILES, J. W. 1988 The evolution of a weakly nonlinear, weakly damped, capillary–gravity wave packet. *J. Fluid Mech.* **187**, 141–154.

NAYFEH, A. H. 1970 Finite amplitude surface waves in a liquid layer. *J. Fluid Mech.* **40**, 671–684.

NAYFEH, A. H. & SARIC, W. S. 1972 Nonlinear waves in a Kelvin–Helmholtz flow. *J. Fluid Mech.* **55**, 311–327.

PEREGRINE, D. H. 1983 Water waves, nonlinear Schrödinger equations and their solutions. *J. Austral. Math. Soc.* B **25**, 16–43.

PERLIN, M. & HAMMACK, J. 1991 Experiments on ripple instabilities. Part 3. Resonant quartets of the Benjamin–Feir type. *J. Fluid Mech.* **229**, 229–268.

PERLIN, M. & TING, C.-L. 1992 Steep gravity–capillary waves within the internal resonance regime. *Phys. Fluids* A **4**, 2466–2478.

PIERSON, W. J. & FIFE, P. 1961 Some nonlinear properties of long-crested periodic waves with lengths near 2.44 centimeters. *J. Geophys. Res.* **66**, 163–179.

POULIQUEN, O., CHOMAZ, J. M., HUERRE, P. & TABELING, P. 1992 Wave-number selection and phase solitons in spatially forced temporal mixing layers. *Phys. Rev. Lett.* **6**, 2596–2599.

PULLIN, D. I. & GRIMSHAW, R. H. J. 1985 Stability of finite-amplitude interfacial waves. Part 2. Numerical results. *J. Fluid Mech.* **160**, 317–336.

RAYLEIGH, LORD, 1915 Deep water waves, progressive or stationary, to the third order of approximation. *Proc. R. Soc. Lond.* A **91**, 345–353.

REEDER, J. & SHINBROT, M. 1981*a* On Wilton ripples, I: formal derivation of the phenomenon. *Wave Motion* **3**, 115–135.

REEDER, J. & SHINBROT, M. 1981*b* On Wilton ripples, II: rigorous results. *Arch. Rat. Mech. Anal.* **77**, 321–347.

SAFFMAN, P. G. & YUEN, H. C. 1982 Finite-amplitude interfacial waves in the presence of a current. *J. Fluid Mech.* **123**, 459–476.

SCHWARTZ, L. W. & VANDEN-BROECK, J.-M. 1979 Numerical solution of the exact equations for capillary–gravity waves. *J. Fluid Mech.* **95**, 119–139.

SIMMONS, W. F. 1969 A variational method for weak resonant wave interactions. *Proc. R. Soc. Lond.* A **309**, 551–575.

THORPE, S. A. 1969 Experiments on the instability of stratified shear flows: immiscible fluids. *J. Fluid Mech.* **39**, 25–48.

TOLAND, J. F. & JONES, M. C. W. 1985 The bifurcation and secondary bifurcation of capillary–gravity waves. *Proc. R. Soc. Lond.* A **399**, 391–417.

VANDEN-BROECK, J.-M. 1980*a* Advances in the numerical computation of capillary–gravity waves. In *Nonlinear partial differential equations in engineering and applied science, Proc. ONR Conf.*, pp. 299–310.

VANDEN-BROECK, J.-M. 1980*b* Numerical calculation of gravity–capillary interfacial waves of finite amplitude. *Phys. Fluids* **23**, 1723–1726.

VANDEN-BROECK, J.-M. 1984 Nonlinear gravity–capillary standing waves in water of arbitrary uniform depth. *J. Fluid Mech.* **139**, 97–104.

WILTON, J. R. 1915 On ripples. *Phil. Mag.* **29**, 688–700.

ZHOU, C. P., LEE, J. H. W. & CHEUNG, Y. K. 1992 Instabilities and bifurcations of interfacial water waves. *Phys. Fluids* A **4**, 1428–1438.